EVALUATION OF THE EFFECTS OF CONVECTION ON PLUME BEHAVIOUR IN THE AOSERP STUDY AREA

by

AKULA VENKATRAM

for

ALBERTA OIL SANDS ENVIRONMENTAL RESEARCH PROGRAM

AS 4.2.6

July 1980

TABLE OF CONTENTS

TABLE OF CONTENTS (CONCLUDED)

LIST OF TABLES

LIST OF FIGURES

ABSTRACT

This report examines the effect of convective turbulence on the dispersion of pollutants emitted from tall stacks in the AOSERP area. As an introduction to this subject the structure of the convective boundary layer is described. Recent models to account for the effects of convection on plume rise are then presented.

The body of this report is devoted to a new model to describe dispersion under convective conditions when tall stacks are most likely to cause significant groundlevel concentrations. The model is applied to the Suncor and Syncrude stacks for selected meteorological conditions. In this connection, the relationship between model predictions and short-term observations is examined in some detail. Finally, suggestions for a field study to verify the model are provided.

ACKNOWLEDGEMENTS

I would like to thank A. Mann and W. Hume of Alberta Environment for providing information and valuable advice through the course of this study.

Thanks are due to Gisela Birmingham for typing this manuscript.

This research project AS 4.2.6 was funded by the Alberta Oil Sands Environmental Research Program, established to fund, direct, and co-ordinate environmental research in the Athabasca Oil Sands area of northeastern Alberta.

1. INTRODUCTION

1.1 TALL STACKS

The obvious reason for using a tall stack to emit pollutants lies in the relationship between the maximum groundlevel concentration C_{max} and the effective stack height h_e. When the plume is brought down to the ground under high wind conditions, C_{max} is inversely proportional to h_e^2. The less obvious but more important advantage of the tall stack is related to the fact that pollutants emitted above the boundary layer do not reach groundlevel for distances relevant to local air quality. For example, the nocturnal boundary layer rarely exceeds 100 m. So it is possible to avoid local air quality problems during nights by releasing pollutants above this height. Present day stacks, which are usually around 200 m, can effectively emit pollutants above the shear generated boundary layer even during the daytime. On the other hand, convective turbulence generated during sunny days usually extends to heights around 1000 m. Normally, economic reasons do not allow stacks to be built this high. Therefore, elevated plumes are invariably affected by the unstable boundary layer. The vigorous turbulence of the planetary boundary layer (PBL) gives rise to large amplitude up and down motion of the plume. "Looping" is the graphical term used to describe this behaviour. Groundlevel concentrations are relatively high during these conditions.

Recent progress in the understanding of the convective boundary layer (Wyngaard et al. 1974; Deardorff 1972) has been accompanied by the development of several models for dispersion of elevated plumes in unstable conditions. Based on physical modelling in a water tank, Deardorff and Willis (1975) proposed one such model. More recently, Lamb (1978) suggested an alternative dispersion parameterization based on the results of numerical simulation. Both these models assume passive releases. Thus, they are not directly applicable to "real" releases which are usually very buoyant. Venkatram (1980a) proposed a model which solves this problem and also incorporates some of the ideas suggested by Deardorff and Willis (1975), Lamb (1978) and Briggs (1975). Its formulation relies heavily on actual groundlevel concentration measurements. Therefore, it is believed that it represents a field-tested operational tool to estimate concentrations caused by elevated sources in convective conditions (see Venkatram and Vet 1979; Venkatram 1980a).

With the modelling experience described above, it is now possible to look at the effects of convective turbulence on plumes in the AOSERP area. Note that the two major sources in the area are over 100 m tall and are thus likely to cause problems when the PBL is unstable. As shall be seen later, the meteorology of the Alberta Oil Sand Environmental Research Program (AOSERP) area (see Figure 1) during summer is conducive to the formation of buoyancy dominated boundary layers. This clearly points to the importance of the subject matter of this report.

1.2 REPORT OUTLINE

The broad objective of this report, namely to study the effects of convection on plume behaviour in the AOSERP area, will be fulfilled within the framework of the following sections.

1. Section 2. In this section, the structure of atmospheric turbulence in the convective boundary layer will be examined. The so-called free convection

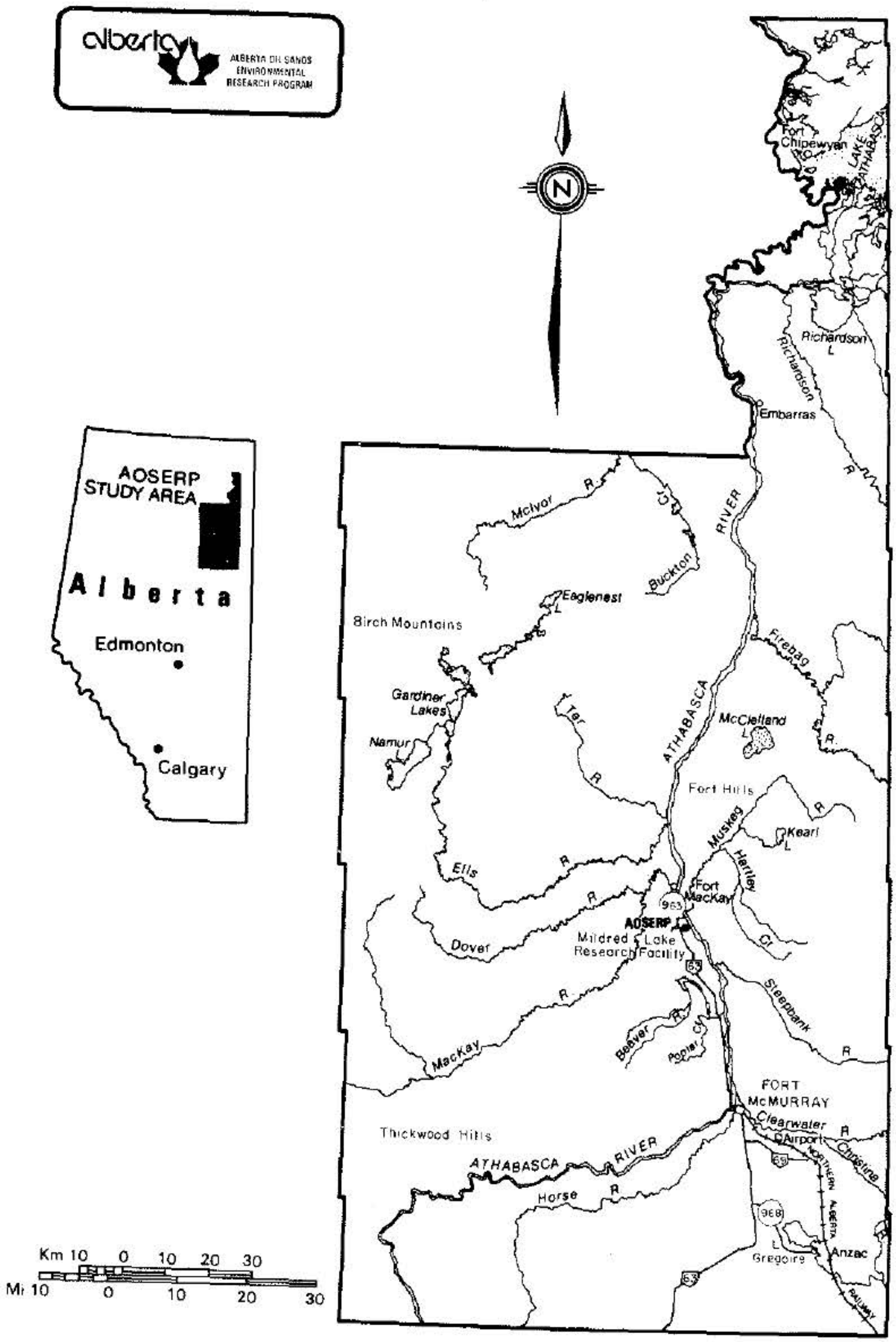

Figure 1. Location of the AOSERP study area.

scales will be derived and it will be seen how they are related to the statistics of buoyancy generated turbulence. These turbulence statistics will be related to the mechanism of dispersion in the convective PBL. Simple models will also be studied to predict the temporal variation of the mixed layer (convective PBL). This predictive capability is important in dispersion modelling.

2. Section 3. Groundlevel concentrations are very sensitive to the extra height added to the stack height by plume buoyancy. In this section, the role of plume behaviour embodied in the 2/3 law can be adapted to describe the motion of plumes in the unstable boundary layer. The "touchdown" equation, which plays an important part in later sections, is derived. Other aspects of the effects of convective turbulence on plume "rise" are examined in some detail.

3. Section 4. This section describes the dispersion model relevant to plumes emitted in the upper part of the convective boundary layer. It is shown how the mean impingement distance obtained from the "touchdown" equation is related to the statistics of plume impingement at groundlevel. Plume spread descriptions suggested by studies of Willis and Deardorff (1976) are then combined with the statistics of plume impingement to yield a simple dispersion model. A brief description is given of

how the model was tested with field data. The model is used to predict groundlevel concentrations expected to be caused by emissions from the two major AOSERP point sources: the Suncor and Syncrude stacks. The relationship between model predictions and measured concentrations is discussed in some detail. This important subject is highlighted by computing the probability of exceeding the Alberta 0.5 h standard of 520 $\mu g.m^{-3}$ for chosen meteorological and stack conditions.

A model is of little value if it has not been tested with field data. To emphasize this aspect of modelling, a possible field study is described to obtain data for model "validation". In this connection, the importance of making measurements compatible with model requirements is demonstrated.

2. GENERAL STRUCTURE OF THE CONVECTIVE BOUNDARY LAYER

2.1 INTRODUCTION

When the turbulence in the boundary layer is maintained largely by buoyant production, the boundary layer is said to be convective or unstable. The source of buoyancy is the upward heat flux originating from the ground heated by incoming solar radiation. In mid-latitudes, the convective boundary layer typically reaches a height of 1 to 2 km by mid-afternoon. This layer is often capped by a sharp inversion which delineates it from the stable turbulence-free layer above it. Convective turbulence is relatively vigorous and causes rapid mixing of the PBL. This thorough mixing gives rise to near-constant distributions of wind and potential temperature. It is now possible to understand why the term "mixed layer" is used synonymously with the convective boundary layer in much of the literature on the subject.

2.2 FREE CONVECTION VARIABLES (see Appendix 7.1)

Figure 2 illustrates the typical structure of the convective boundary layer. Observations (Kaimal et al. 1976) indicate that all of the potential temperature change occurs in a very shallow region close to the ground. Nearly all the wind shear also is confined to this layer. Following Kaimal et al. (1976), the boundary layer is idealized as a three-layer system.

2.2.1 The Surface Layer

Wind shear plays the dominant role in the surface layer. According to Monin-Obukhov's similarity theory, the turbulent structure in this layer is determined by the group u_*, H_o, z and g/T, where u_* is

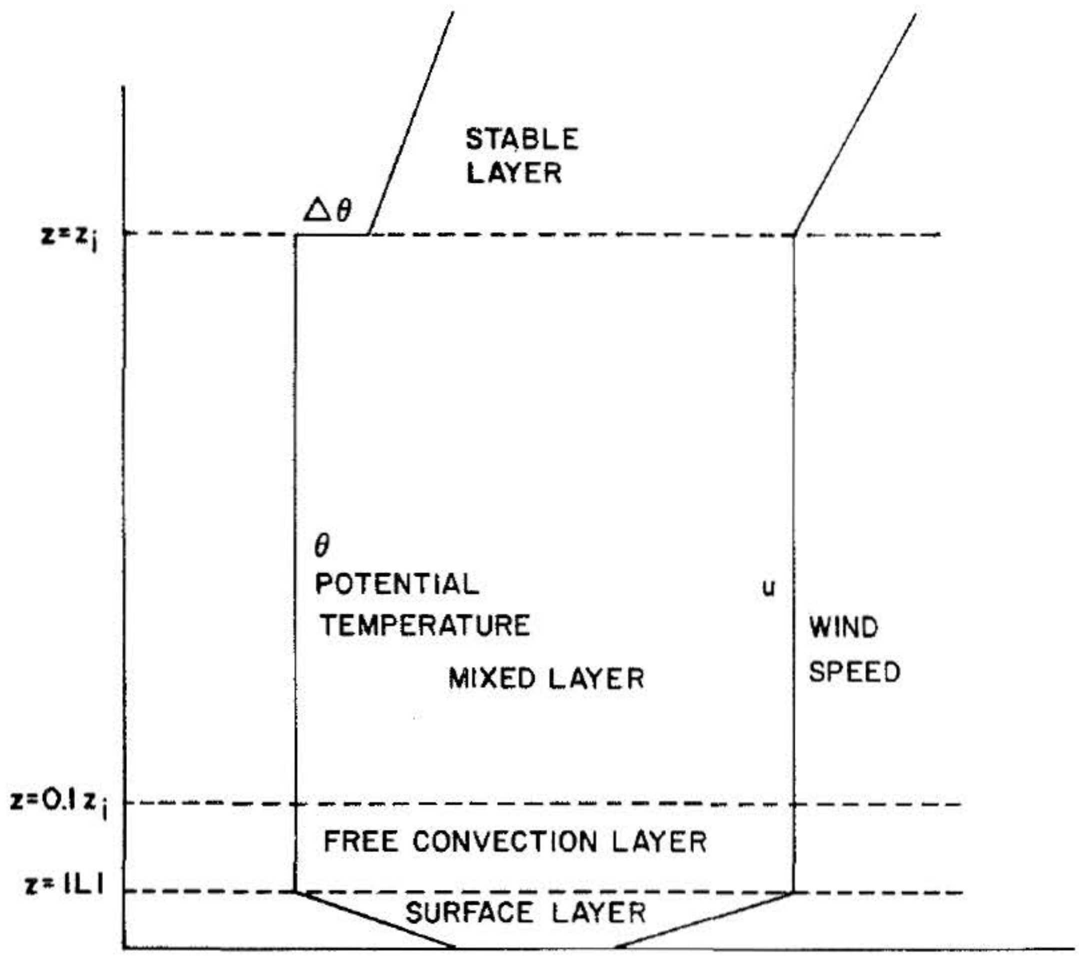

Figure 2. Typical profiles of potential temperature and wind speed in the mixed layer.

the surface friction velocity, H_o is the surface kinematic heat flux, z is the vertical distance from the ground and g/T is the buoyancy parameter. To illustrate this idea, let us consider the expression for the vertical velocity variance $\overline{w'^2}$

$$\overline{w'^2} = f(u_*, H_o, z, g/T) \tag{1}$$

Using dimensional analysis, equation (1) is rewritten as

$$\frac{\overline{w'^2}}{u_*^2} = f_2(z/L) \tag{2}$$

where L the Monin-Obukhov length is given by

$$L \equiv \frac{-u_*^3 T}{kgH_o} \tag{3}$$

Equation (2) tells us that $\overline{w'^2}$ when "scaled" by u_*^2 is a universal function of z/L regardless of the conditions under which it is measured. To extend this a little further, the appropriate velocity and temperature scales for the surface layer are defined as (Wyngaard 1973)

$$\begin{aligned} &\text{Velocity} \quad u_* \equiv (\tau_o/\rho)^{1/2} \\ &\text{Temperature} \ T_* \equiv -H_o/u_* \end{aligned} \tag{4}$$

Then, the Monin-Obukhov similarity hypothesis states that suitable surface layer variables when non-dimensionalized by these scales are only functions of z/L. A number of recent experiments (see Kaimal et al. 1976) support this behaviour for most boundary layer variables with the exception of the u' and v' turbulent velocities. More will be said about the horizontal velocity components in a later section. The surface layer is confined to $z < |L|$.

2.2.2 Free Convection Layer

The shear stress τ_o is no longer important in the free convection layer. The boundary layer variables are governed by the group H_o, z and g/T which yield the scaling velocity u_f and the scaling temperature T_f given by

$$u_f = \left[H_o z(g/T)\right]^{1/3} \tag{5}$$

$$T_f = H_o/u_f \tag{6}$$

Dimensional analysis tells one that

$$\overline{w'^2} \propto u_f^2 \text{ and } \overline{\theta'^2} \propto T_f^2 \tag{7}$$

where $\overline{\theta'^2}$ is the temperature variance. In terms of M-O variables, equation (7) can be rewritten as

$$\overline{w'^2}/u_*^2 \propto (-z/L)^{2/3} \tag{8}$$

$$\overline{\theta'^2}/T_*^2 \propto (-z/L)^{-2/3} \tag{9}$$

It can be seen from equations (8) and (9) that the velocity fluctuations are greater and the temperature fluctuations less than at neutral ($z/L \simeq o$) by the factor $(-z/L)^{1/3}$. These scaling laws are well supported by the Kansas data (Wyngaard et al. 1971) and explicit expressions can be written for the standard deviations of the vertical velocity and temperature fluctuations as follows,

$$\sigma_w = 1.33(gH_oz/T)^{1/3} \tag{10a}$$

$$\sigma_\theta = 1.35\ H_o^{2/3}(gz/T)^{-1/3} \tag{10b}$$

Note that equation (10b) suggests a simple method of obtaining the surface heat flux H_o. The quantity σ_θ can be measured using relatively simple fast response temperature sensors. Thus using H_o derived from equation (10b), it is possible to compute σ_w through equation (10a). Direct measurement of σ_w in the free convection layer is difficult because of averaging problems which are described by Wyngaard (1973).

Note that σ_w determines the vertical dispersion of a plume. For a stack emitting well above the surface layer, the best method of determining the σ_w controlling dispersion of the plume is to use an aircraft to measure σ_θ and hence σ_w. The main advantage of this method is that the aircraft "sees" an area averaged σ_w which is more relevant to the dispersion of an elevated plume than that derived from a ground based point measurement.

As in the surface layer, M-O similarity theory does not apply to the horizontal velocity fluctuations. In fact, observations indicate that (Kaimal et al. 1976)

$$\sigma_\alpha = Cw_* \ ; \ \alpha = u,v \tag{11}$$

where $C = 0.6$ and w_* is the convective velocity scale given by

$$w_* \equiv \left[(g/T)H_oz_i\right]^{1/3} \tag{12}$$

In equation (12), z_i is the thickness of the mixed layer. Panofsky et al. (1977) show that equation (11) extends all the way down into the surface layer. A plausible physical explanation for this behaviour is that the horizontal velocity fluctuations in the surface layer are dominated by large eddies which extend through the depth of the mixed layer. These eddies, whose velocities scale with w_*, have more nearly horizontal motion in the surface layer and thus contribute little energy to the vertical velocity fluctuations.

The results of the Minnesota study in 1973, reported by Kaimal et al. (1976), indicate that the upper limit of the free convection layer is approximately $0.1\ z_i$. So for a typical mixed layer height of 1000 m, the free convection layer would be given by the limits $|L| < z < 100$ m.

2.2.3 Mixed Layer

The region above $0.1\ z_i$ is referred to as the mixed layer where the structure of turbulence is dependent on z_i and the group H_o, g/T and z_i determines the velocity scale w_* and the temperature scale θ_* given by

$$w_* = \left[(g/T) H_o z_i\right]^{1/3} \tag{13a}$$

$$\theta_* = H_o / w_* \tag{13b}$$

In the mixed layer, it is expected that dimensionless groups formed with w_* and θ_* be functions of z/z_i. For example, the standard deviation of the vertical velocity fluctuation σ_w would be given by

$$\frac{\sigma_w}{w_*} = f\left(\frac{z}{z_i}\right) \tag{14}$$

Mixed layer scaling is supported by results of model studies (Deardorff 1972) as well as observations

(Kaimal et al. 1976). From the point of view of dispersion, it is useful to know that $\sigma_w \simeq 0.6w_*$ in the region $0.1\ z_i < z < z_i$; σ_v is also approximately $0.6w_*$. Clearly, this behaviour of the turbulent velocity fluctuations simplifies the modelling of elevated releases in the mixed layer.

2.3 EVOLUTION OF THE CONVECTIVE BOUNDARY LAYER

It is assumed by the present author that the convective boundary layer is horizontally homogeneous and stationary. As the boundary layer grows in response to the heating at the earth's surface, the assumption of stationarity implies that the turbulence can be considered to follow a sequence of equilibrium states. This assumption can be crudely justified as follows. For a typical $z_i = 1000$ m and $w_* = 1\ \text{ms}^{-1}$, the relevant mixing time scale z_i/w_* works out to be around 1000 s. This is small compared to the time scales of surface heat flux variation which Wyngaard (1973) estimated to be around 4 h at midday. This means that, around the noon hour, the turbulence structure reacts rapidly enough to be in equilibrium with the "slowly" varying forcing at the surface. More will be said about this later on in this section.

As the length scales are of the order of z_i above the surface layer, it is expected that the averaging effect of the turbulent mixing will filter out surface inhomogeneities with scales less than z_i. This intuitive argument tells us that the convective boundary layer can be considered to be horizontally homogeneous over distances comparable to z_i. Thus, it should be possible to ignore fine scale surface features affecting the sensible heat flux. This also points to the necessity to use the type of technique suggested earlier to measure the z_i averaged heat flux controlling the evolution of the boundary layer.

It is evident that it is necessary to know the time variation of the boundary layer in order to be able to predict the behaviour of an elevated plume. In this section, a simple model for the dynamics of the convective boundary layer will be described. For the type of information required for modelling dispersion a more sophisticated description is not required. In the present model, it is assumed that the gradients of potential temperature and velocity are confined to a layer whose thickness is negligible compared to z_i. Also the inversion layer which separates the convective boundary layer from the non-turbulent stable atmosphere above is taken to be thin enough to be represented by a step discontinuity in the potential temperature. In Figure 3, the potential temperature gradient in the stable layer is seen to be independent of height. As shown by Venkatram (1977), this is not a necessary assumption as the model can handle changes in γ.

For this simple model of the mixed layer, the thermal energy equation can be written as (Carson 1973)

$$z_i \frac{d\theta_m}{dt} = H_o - H_i \tag{15a}$$

and

$$\frac{dz_i}{dt} = w_i - \frac{H_i}{\Delta\theta} \tag{15b}$$

where θ_m is the potential temperature of the mixed layer, $\Delta\theta$ is the temperature jump across the inversion, and H_i is heat flux at the inversion base. For simplicity, the vertical velocity w_i at the top of the mixed layer will be neglected.

To close the set of equations we require an expression for H_i or equivalently $\Delta\theta$. The following simple closure equation suggested by Plate (1972) will

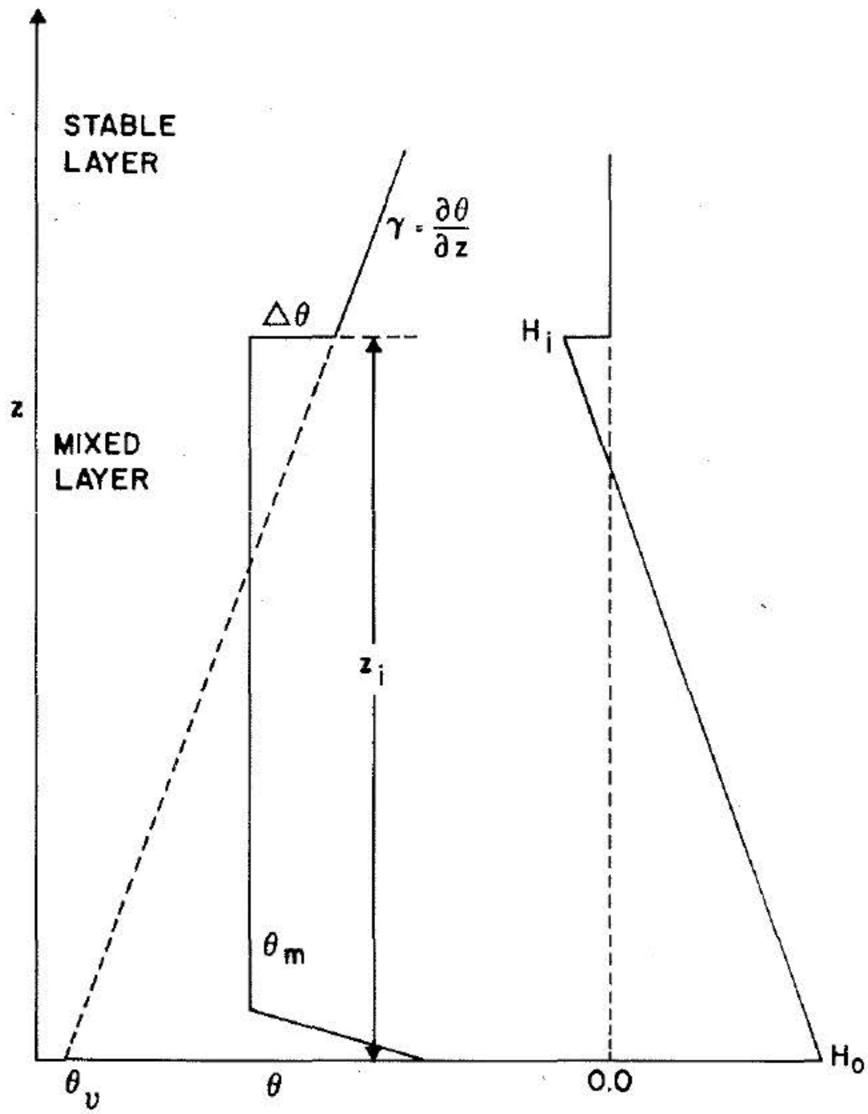

Figure 3. Representation of idealized potential temperature and heat flux profiles in the mixed layer.

be used

$$\Delta\theta = f\gamma z_i \tag{16}$$

where f is a constant less than 1. By combining equations (15) and (16), it can be readily shown that the closure assumption is equivalent to the commonly used expression (Carson 1973)

$$H_o = -AH_i \tag{17a}$$

$$A \equiv f/(1 - 2f) \tag{17b}$$

Carson (1973) indicates that equation (17) is not satisfactory as A varies during the evolution of the mixed layer. However, this is not critical as estimates of mixed layer height using equation (17) have compared very favourably with observations (Tennekes and van Ulden 1974). Furthermore, Mahrt and Lenschow (1976) show that, for a typical variation of A from 0.15 to 0.25 the corresponding change in the mixed layer height is only 7%. Additional justification for this assertion is provided in Venkatram (1977).

Referring to Figure 3, the mixed layer depth z_i can be expressed as follows

$$z_i = (\theta_m - \theta_v)/\gamma(1 - f) \tag{18}$$

where θ_v is the temperature obtained by extrapolating the stable profile above the mixed layer to the earth's surface. The equation for the growth of z_i can now be written as

$$z_i^2 = z_i^2(o) + \frac{2}{\gamma(1 - 2f)} \int_o^t H_o(t)dt \tag{19}$$

where t = o corresponds to sunrise. Equation (19) can be integrated if one approximates the variation of H_o by the sine function $H_o = H_m \sin(\pi t/2\tau)$ where τ is roughly half the time period between sunrise and sunset. It should be mentioned that observations (Wyngaard 1973) support this assumed behaviour of the surface heat flux. Integration of equation (19) yields

$$z_i^2(t) = z_i^2(o) + \left[\frac{8\tau H_m}{\pi\gamma(1 - 2f)}\right] \sin^2(\frac{\pi t}{4\tau}) \qquad (20)$$

The initial $z_i(o)$ corresponds to the nocturnal boundary layer height which is normally around 100 m. It is seen from equation (20) that the relative error associated with neglecting $z_i(o)$ is $[1 - (z_i(o)/z_i(t))^2]^{1/2}$. This suggests that for most practical purposes $z_i(o)$ is not important. For example, if $z_i(t) = 400$ m and $z_i(o) = 100$ m, the mixing height obtained by neglecting $z_i(o)$ will be 387 m which differs from the actual value by only 3%. Then the explicit expression for $z_i(t)$ becomes

$$z_i(t) = \left[\frac{8\tau H_m}{\pi\gamma(1 - 2f)}\right]^{1/2} \sin(\frac{\pi t}{4\tau}) \qquad (21)$$

Note that z_i grows as long as there is energy input into the boundary layer and reaches a maximum at $t = 2\tau$ around sunset.

With equation (21), it is worthwhile to derive an expression for w_* which is the relevant velocity scale for turbulent fluctuations in the convective boundary layer. The definition of w_* (equation 12) yields

$$w_* = (\frac{g}{T})^{1/3} 2^{5/6} \left[\frac{\tau}{\pi\gamma(1-2f)}\right]^{1/6} \sin^{2/3}(\frac{\pi t}{4\tau}) \cos^{1/3}(\frac{\pi t}{4\tau}) H_m^{1/2} \qquad (22)$$

It can be noted from equation (22) that the 1/6 power dependence of w_* on γ and f implies that the time of day essentially determines w_*. This means that w_* can be computed by estimating Q_m.

As high concentrations associated with looping usually occur when convective activity is highest, it is instructive to calculate the maximum value of w_*. From equation (22) the maximum can be seen to occur at $t = 1.22\ \tau$ and is given by

$$w_{*m} = \left(\frac{g}{T}\right)^{1/3} \frac{2^{7/6}}{\sqrt{3}} \left(\frac{\tau}{\pi\gamma(1 - 2f)}\right)^{1/6} H_m^{1/2} \qquad (23)$$

The weak dependence of w_* on γ, f and τ can be exploited by assigning typical values to these variables and computing the "constant" associated with $H_m^{1/2}$. By taking $\gamma = 5 \times 10^{-3}$ C m^{-1}, f = 1/7 and τ = 8 hr, possibly corresponding to summer in the AOSERP area,

$$w_{*m} = 4.85\ H_m^{1/2} \qquad (24)$$

where the units of H_m are ms^{-1}C.

Similarly, w_{*m} can be related to the maximum mixed layer height z_{im} through the equation

$$w_{*m} = 0.46 \left[\frac{\pi\gamma(1 - 2f)}{\tau}\right]^{1/3} \left(\frac{g}{T}\right)^{1/3} z_{im} \qquad (25)$$

Equation (25) shows that w_{*m} is more sensitive to γ and τ if z_{im} is used rather than H_m to estimate w_{*m}. With the values of γ, f and τ used before, w_{*m} reduces to

$$w_{*m} = 1.07 \times 10^{-3}\ z_{im} \qquad (26)$$

In writing equations (24) and (25), it is not implied that the "constants" in them are real in the usual sense. Instead, the relatively weak dependence of w_{*m} on γ, f and τ probably allows the use of "typical" values of these PBL variables to estimate w_{*m}. For example, an extreme factor of 4 variation in γ translates into a 26% change in w_{*m}. Thus, with the more normal changes in γ, the estimate of w_* from a relationship of the type given in equation (24) should be sufficiently accurate for air pollution applications. This expectation is borne out in an analysis of the Minnesota data (Kaimal et al. 1976) by Venkatram (1978).

At this point, it is useful to illustrate the use of the equations derived by applying them to the AOSERP area. H_m will be estimated by assuming that it is proportional to the incoming solar radiation at the earth's surface. Then following Briggs (1975), it can be written as

$$H_m = AS_I/\rho C_p; \; S_I = \frac{2}{3} \sin \theta_{el}(1 - 0.8C)S \qquad (27)$$

where in (27), S_I is the incoming solar radiation, θ_{el} is the maximum solar elevation angle on the day of interest, C is the fractional cloudiness, S is the solar constant, and ρC_p corresponds to air. The constant A is a function of ground cover, and it varies from 0.25 for a crop canopy to 0.55 for a dry surface. It can be determined by calibrating measured heat fluxes against incoming solar radiation. The maximum solar elevation angle can be written as

$$\sin \theta_{el} = \sin \lambda \sin \delta + \cos \lambda \cos \delta \qquad (28)$$

where λ is the latitude and δ is the declination corresponding to the time of observation. For the AOSERP area, λ will be taken to equal 57°, and w_{*m} will be computed for the months May to September, during which time the ground is typically free of snow (Longley and Janz 1979). Table 1 presents the variation of w_{*m} and z_i during these months. Note that w_{*m} would roughly correspond to the average value of w_* during the noon hours. As the AOSERP area has considerable cloudiness during most of the year (Longley and Janz 1979), w_{*m} and z_i have also been computed for C = 0.7 which is the average value for the area of interest. It is noted from Table 1 that there is vigorous convective activity during the daytime hours of the months extending from May to September. The convective velocity scale w_* can be over 2 $m.s^{-1}$ during the noon hours. Recall that $\sigma_w \simeq 0.6\ w_*$ so that the vertical velocity fluctuations can be over 1 $m.s^{-1}$. The mixed layer height z_i is expected to be over 1000 m during the majority of the daytime hours considered. This information on the typical values of w_* and z_i will be useful in assessing the results seen in later sections.

2.4 CONDITIONS FOR THE APPLICABILITY OF CONVECTIVE SCALING

A reasonable measure of the degree of convective activity in the PBL is the ratio $|L|/z_i$ which can be expressed as

$$\frac{|L|}{z_i} = \left(\frac{u_*}{w_*}\right)^3 \frac{1}{k} \qquad (29)$$

It is seen that the ratio indicates the relative magnitudes of the turbulent velocities produced by shear and buoyancy. The role played by shear can be made more clear by determining the Monin-Obukhov length L for specified values of the mixed layer wind u. This task is accomplished by using the convective drag law proposed by Wyngaard et al. (1974)

Table 1. Variation of w_{*m} and z_i during the summer months. The numbers in the parenthesis correspond to fractional cloudiness of 0.7. The declination angles (δ) used correspond to the beginning of the month. Parameters used in the computation are $\tau = 8$ h, $\gamma = 5$ C/1000 m, $f = 1/7$.

Month	H_m $m.s^{-1}C$	$w_{*m}(C = 0.0)$ $m.s^{-1}$	$w_{*m}(C = 0.7)$ $m.s^{-1}$	$z_i(t = 1.22\ \tau)$ m
May	0.24 (0.11)	2.38	1.61	1820 (1230)
June	0.26 (0.11)	2.47	1.61	1900 (1230)
July	0.26 (0.11)	2.47	1.61	1900 (1230)
August	0.25 (0.11)	2.43	1.61	1850 (1230)
September	0.21 (0.09)	2.22	1.46	1700 (1120)

$$\frac{u}{u_*} = \frac{1}{k} \ln\left(\frac{-L}{z_o}\right) \tag{30}$$

For chosen values of H_o, u and z_o one can compute u_* and hence L through its definition. Table 2 shows the results of this calculation for various combinations of H_m and u. The value of z_o of 1 m is representative of the forested AOSERP area. The use of a constant u, although not very realistic, should not affect the main conclusions of the following analysis.

The PBL is considered convective when $z_i > 10\ |L|$. Under these conditions thermal plumes remain undistorted by shear (Deardorff, 1974). It is seen from Table 1 that at $u = 5\ m.s^{-1}$ and $H_m = 0.2\ m.s^{-1}C$, the PBL is convective during the period $0.4 < t < 1.8$. More than 9/10th of the boundary layer is dominated by buoyancy generation of turbulence. It is recalled that σ_w varies as $z^{1/3}$ in the region $|L| < z < 0.1\ z_i$. However, as σ_w appears in the form $\sigma_w/u(z)$ in dispersion formulations (see later sections), there should be little error involved in assuming that w_* is the relevant velocity scale for $z > |L|$. The justification for this is that u(z) decreases with height so that $\sigma_w/u(z) \propto w_*/u$.

When u is increased to $10\ m.s^{-1}$, the effects of shear are important for $\overline{t} < 1.0$ after which time the PBL becomes convective. For $u = 5\ m.s^{-1}$ and $H_m = 0.1\ m.s^{-1}\ C$ the boundary layer is dominated by buoyancy for $\overline{t} > 0.6$.

There is strong empirical evidence (see Venkatram 1980a) to indicate that convective velocity scaling is appropriate whenever $|L|$ is less than the effective stack height. In other words, the criterion $z_i > 10\ |L|$ does not appear to be very stringent as far as the estimation of concentrations is concerned. The

Table 2. Variation with time of selected meteorological parameters $\bar{t} = t/\tau$ where t is the time and τ is the half-period of the surface heat flux.

1. $u = 5\ m.s^{-1}$, $H_m = 0.2\ m.s^{-1}C$, $z_o = 1.0\ m$

$\bar{t}$	0.20	0.40	0.60	0.80	1.00	1.20	1.40	1.60	1.80
z_i (m)	317.00	626.00	920.00	1191.00	1433.00	1640.00	1807.00	1927.00	2001.00
u_* $(m.s^{-1})$	0.39	0.43	0.45	0.46	0.46	0.46	0.45	0.43	0.39
-L (m)	86.00	59.00	49.00	45.00	44.00	45.00	49.00	59.00	86.00
w_* $(m.s^{-1})$	0.85	1.34	1.70	1.95	2.08	2.16	2.13	1.95	1.58

2. $u = 10\ m.s^{-1}$, $H_m = 0.2\ m.s^{-1}$, $z_o = 1.0\ m$

$\bar{t}$	0.20	0.40	0.60	0.80	1.00	1.20	1.40	1.60	1.80
z_i (m)	317.00	626.00	920.00	1191.00	1433.00	1640.00	1807.00	1927.00	2001.00
u_* $(m.s^{-1})$	0.61	0.66	0.68	0.70	0.70	0.70	0.68	0.66	0.61
-L (m)	317.00	209.00	171.00	154.00	149.00	154.00	171.00	209.00	317.00
w_* $(m.s^{-1})$	0.85	1.34	1.70	1.95	2.08	2.16	2.13	1.95	1.58

continued...

Table 2. Concluded.

3. $u = 5\ m.s^{-1}$, $H_m = 0.1\ m.s^{-1}C$, $z_o = 1.0\ m$

$\bar{t}$	0.2	0.4	0.6	0.80	1.00	1.20	1.40	1.60	1.80
z_i (m)	224.00	443.00	651.00	842.00	1013.00	1159.00	1277.00	1363.00	1415.00
u_* $(m.s^{-1})$	0.36	0.39	0.41	0.42	0.42	0.42	0.41	0.39	0.36
$-L$ (m)	131.00	88.00	73.00	67.00	64.00	67.00	73.00	88.00	131.00
w_* $(m.s^{-1})$	0.61	0.95	1.21	1.39	1.50	1.54	1.51	1.38	1.13

author believes that convective turbulence is likely to control dispersion during most of the daytime hours when the heat flux is away from the ground. As the winds are generally light in the AOSERP area there is good reason to pay more attention to dispersion governed by buoyancy generated turbulence. A preliminary study by Strosher and Peters (1980) describes the situations under which convective activity affects dispersion of the plumes in the AOSERP region.

3. PLUME RISE

3.1 PLUME RISE IN NEUTRAL CONDITIONS

A simple derivation of plume rise in a neutral atmosphere will be given in this section. For a more detailed rigorous derivation, the reader is referred to the excellent monograph by Briggs (1975). Although the present discussion will appeal to intuition, it will emphasize the physics required for a clear understanding of the convective dispersion model described in a later section.

Following Csanady (1956) it will be assumed that the plume spread is dominated by self-generated turbulence. Turbulence outside the plume is neglected. Observations (Briggs 1975) indicate that internal turbulence produces a near uniform profile of concentration and temperature across a fairly defined plume cross-section. Thus the top-hat assumption is appropriate here and it is possible to describe the geometry of the plume by a single parameter r corresponding to the radius of the plume. The plume is assumed to rise through an atmosphere with uniform profiles of potential temperature and velocity. Note that this assumption is appropriate for the convective PBL. For the bent-over phase, it will be assumed that the plume travels at the wind speed u (see Briggs 1975). Figure 4 shows a schematic of the physical system being considered.

The thermal energy equation for the plume can be written as

$$\frac{d\theta}{dt} = -\frac{\partial}{\partial x_i}\overline{(\theta' u_i')} \qquad (32)$$

where θ is the potential temperature and the subscript 'p'

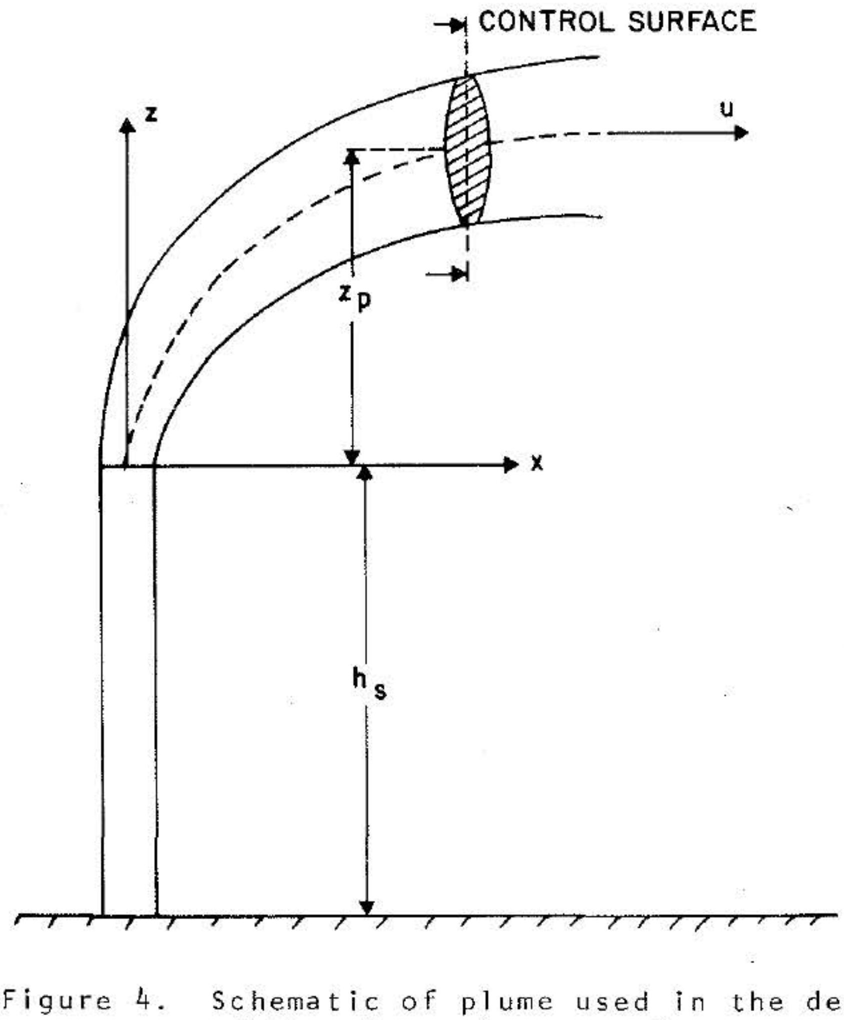

Figure 4. Schematic of plume used in the derivation of the plume rise equation.

will refer to the plume. The primed quantities refer to turbulent fluctuations. If equation (32) is integrated across the vertical plane shown in Figure 4, it is found

$$\frac{d}{dt} A(\theta_p - \theta_a) = 0 \tag{33}$$

where θ_a is the constant ambient potential temperature, and A is area of the plume cross-section at time t. The turbulent cross-correlation terms disappear in the integration which extends beyond the plume edges. Integrating equation (33) yields

$$A(\theta_p - \theta_a) = C \tag{34a}$$

or

$$\frac{g}{\theta_a} r^2 u(\theta_p - \theta_a) = F_o \tag{34b}$$

where F_o is the constant buoyancy parameter determined by stack conditions. Briggs (1975) shows that F_o can be approximated by

$$F_o = \frac{g}{T_s} v_s r_s^2 (T_s - T_a) \tag{35}$$

In equation (35), T is the absolute temperature in degrees Kelvin, the subscript 's' refers to stack conditions, and v_s is the exit gas velocity at the stack mouth with radius r_s. Note that equation (34b) can be rewritten as

$$g r^2 u \frac{(T_p - T_a)}{T_a} = F_o \tag{36}$$

Now consider the vertical momentum equation

$$\rho \frac{dw}{dt} = - \frac{\partial p}{\partial z} - \rho g - \frac{\partial}{\partial x_i} \overline{(w' u_i')} \tag{37}$$

Using the hydrostatic assumption, equation (37) can be expressed as

$$\rho\frac{dw}{dt} = (\rho_a - \rho)g - \frac{\partial}{\partial x_i}\overline{(w'u_i')} \qquad (38)$$

Integrating equation (38) across the plume cross-section,

$$\frac{d}{dt}(w_p A) = \frac{A(\rho_a - \rho_p)g}{\rho_p} \qquad (39)$$

With the relationship $p = \rho RT$ and assuming that p does not vary across A, equation (39) can be written as

$$\frac{d}{dt}(r^2 w_p) = \frac{gr^2}{T_a}(T_p - T_a) \qquad (40a)$$

or

$$\frac{d}{dt}(r^2 w_p) = \frac{F_o}{u} \qquad (40b)$$

Integrating equation (40b) yields

$$r^2 w_p = \frac{F_o t}{u} + \frac{F_m}{u} \; ; \; F_m \equiv v_s^2 r_s^2 \qquad (41)$$

The second term on the right of equation (41) ensures that vertical momentum is conserved within the Boussinesq approximation. To proceed further, it will be assumed that the rate of growth of the plume radius is proportional to the vertical velocity of the plume,

$$\frac{dr}{dt} = \beta w_p \equiv \beta\frac{dz_p}{dt} \qquad (42)$$

In equation (42), β is an entrainment constant whose value has been found to be 0.6 from observations (see Briggs 1975 for details). Substituting equation (42) into equation (41) and integrating with the initial condition r = o, t = o, it is seen that

$$r = \left[\left(\frac{3}{2}\beta \frac{F_o}{u}\right) t^2 + \left(3\beta \frac{F_m}{u}\right) t \right]^{1/3} \qquad (43a)$$

or

$$z_p = \left[\left(\frac{3}{2\beta^2}\right) \frac{F_o}{u} t^2 + \left(\frac{3}{\beta^2}\right) \frac{F_m}{u} t \right]^{1/3} \qquad (43b)$$

For most stacks the buoyancy term in equation (43b) becomes dominant very close to the source (≃50 m). Therefore, in the subsequent discussion the effect of initial momentum on z_p will be neglected.

Clearly the transformation $x = ut$ is not consistent with the initial condition for r. However, for practical purposes the approximation is good and z_p can be expressed as

$$z_p = 1.6 \frac{F_o}{u}^{1/3} x^{2/3} \; ; \; \beta = 0.6 \qquad (44)$$

Equation (44), commonly referred to as '2/3 law' for plume rise, will be used in the convective dispersion model described in a later section.

At this point it is useful to highlight the essential physics of plume rise in an adiabatic atmosphere. It is easy to see that the buoyancy F_b acting upwards on unit mass of a plume is

$$F_b = \frac{g(T_p - T_a)}{T_a} \qquad (45)$$

It can be seen from equation (36) that the flux of buoyancy F_b is conserved in an adiabatic atmosphere,

$$ur^2 F_b = \text{constant} = F_o \qquad (46)$$

To better appreciate the plume rise equations, the 2/3 law will be rederived using a simple physical argument. Dimensional analysis indicates that the vertical velocity w_p of the plume is given by

$$w_p \propto F_b t \tag{47}$$

or

$$\frac{dz_p}{dt} \propto F_b t \tag{48a}$$

or

$$ur^2 \frac{dz_p}{dt} \propto F_o t \tag{48b}$$

Since $r \alpha z_p$ is the only physically plausible scaling relationship, equation (48b) can be written as

$$\frac{dz^3_p}{dt} \propto \left(\frac{F_o}{u}\right) t \tag{49}$$

Integration of equation (49) yields the 2/3 law for plume rise. It is useful to note that

$$w_p \propto \left(\frac{F_o}{u}\right)^{1/3} t^{-1/3} \tag{50}$$

The singularity at $t = o$, associated with the condition $r(t = o) = o$ does not invalidate the plume rise equation.

The 2/3 law for plume rise indicates that the plume will continue to rise until it is broken up by atmospheric turbulence; thus the final plume rise is a strong function of atmospheric turbulence. In view of this, formulations which do not explicitly account for atmospheric turbulence are not physically correct even if they make dimensional sense. The Holland plume rise equation is an example of such a formulation. The effects of atmospheric turbulence will be treated in detail in the next section.

3.2 EFFECTS OF CONVECTION ON PLUME RISE

It is generally assumed (Briggs 1975) that a buoyant plume is dominated by self-induced turbulence until it is abruptly broken up by atmospheric turbulence. Plume rise terminates at this point when the turbulent velocity w_i associated with the plume is comparable to atmospheric velocity fluctuations which is denoted by w_a. Then the "breakup" model of plume rise states that

$$w_i = w_a \text{ at plume "breakup"} \tag{51}$$

As the turbulent circulation in the plume is induced by the relative motion between the atmosphere and the plume rising vertically at a velocity w_p, it is reasonable to assume that $w_i \propto w_p$.

There are two plausible ways to express w_a. The obvious choice for w_a is the standard deviation of the vertical velocity fluctuations σ_w. Then using equation (50) for w_p, the "breakup" equation can be written as

$$\sigma_w \propto \left(\frac{F_o}{u}\right)^{1/3} t_b^{-1/3} \tag{52}$$

where t_b refers to the time of plume termination. Then t_b becomes

$$t_b \propto \frac{F_o}{u\sigma_w^3} \tag{53}$$

Substituting equation (53) into the plume rise equation (44),

$$z_{pf} \propto \frac{F_o}{u\sigma_w^2} \tag{54}$$

where z_{pf} is the final plume rise. If the plume rises through the shear dominated surface layer, $\sigma_w \propto u_*$ in which case

$$z_{pf} \propto \frac{F_o}{uu_*^2} \tag{55}$$

Since $u_* \propto u$, the above equation becomes

$$z_{pf} \propto \frac{F_o}{u^3} \tag{56}$$

For an elevated release into the convective mixed layer, $\sigma_w \propto w_*$ and the final plume rise becomes

$$z_{pf} \propto \frac{F_o}{uw_*^2} \tag{57}$$

Proportionality constants have not been put into the equations for z_{pf} as the observational evidence to fix the constants is virtually nonexistent (Briggs 1975). It should be mentioned, however, that Weil and Hoult (1973) found that model predictions of concentrations compared well with observations when the implied constant in equation (57) was chosen to be unity.

Briggs (1975) believes that a more physically appealing expression for w_a can be formulated by noting that the plume thickness at breakup is usually less than the dominant atmospheric eddy size. If z_p($\propto$ plume diameter) is within the inertial subrange, it can be assumed that the velocity scale of the eddies contributing to the breakup of the plume is proportional to $(\varepsilon\ z_p)^{1/3}$ where ε is the atmospheric dissipation rate at plume height. Then it can be shown (Briggs 1975) that

$$z_{pf} = \left(\frac{2}{3\beta^2}\right)^{3/5} \left(\frac{F_o}{u}\right)^{3/5} \left(\frac{\eta}{\varepsilon}\right)^{2/5} \tag{58}$$

where $\eta = 1.5$ and $\beta = 0.6$. For convective conditions, Briggs (1975) reasons that ε in equation (58) should correspond to downdrafts which bring segments of the plume down to the ground. Using $\varepsilon = 0.25\ gH_o/T$ from Deardorff's (1974) experiments, Briggs reduces equation (58) to

$$z_{pf} = 3\left(\frac{F_o}{u}\right)^{3/5}\left(\frac{g}{T}\ H_o\right)^{-2/5} \tag{59}$$

As noted before, there is little observational confirmation of expressions for z_{pf}. Under neutral conditions (high wind), the plume is usually invisible by the time its rise terminates. Under convective conditions, the large amplitude up and down motion of the plume does not allow for an unambiguous determination of z_{pf}. At the present time, the correctness of the formulations can be tested only indirectly for z_{pf} by comparing concentration predictions derived from them with observed concentrations. This will be discussed in more detail in a later section.

3.3 TOUCHDOWN MODEL

Observations (Kaimal et al. 1976) indicate that turbulent activity in the convective PBL is in the form of long-lived updrafts and downdrafts. The relatively vigorous updrafts originating from the heated ground extend all the way to the top of the mixed layer. The upward motion in the updrafts is compensated by less turbulent subsidence in downdrafts. When the wind is small, these thermal plumes are randomly distributed in space and time. They can also originate between vortex rolls in a PBL with considerable shear across it. In both these situations, the dimensions of these updrafts and downdrafts scale with z_i. Their vertical velocities scale with w_*.

The longevity and coherence of the convective structures in the PBL can give rise to unusual effects. For example, pollutants emitted into a downdraft may continue to travel downward until they impact on the ground. Similarly, a plume segment emitted into an updraft can be carried all the way to the top of the mixed layer. As a downdraft is less turbulent than an updraft, the plume tends to be more coherent when it travels downwards. This causes the locus of maximum concentration to descend from the source. Numerical modeling (Lamb 1979) indicates that for source heights greater than 0.25 z_i this rate of descent is about 0.5 w_*.

With these preliminaries, a simple model can be constructed for plume behaviour in a convective layer. Briggs (1975) suggests that the first stage of plume rise is maintained relative to the motion of a downdraft (or updraft). Then the trajectory of the plume segment would be described by the equation

$$z_p(t) = \frac{\alpha F^{1/3} x^{2/3}}{u} - \frac{w_d x}{u} \tag{60}$$

The first term on the right refers to the familiar 2/3 law while the second term is associated with the downdraft velocity which is denoted by w_d. Then plume touchdown at the ground occurs when $z_p = -h_s$ where h_s is the stack height. The mean plume impingement distance x_i is the solution of the so-called touchdown equation,

$$\frac{\alpha F^{1/3} x_i^{2/3}}{u} - \frac{w_d x_i}{u} = -h_s \tag{61}$$

where $w_d \simeq 0.5\, w_*$. The discussion should not imply that the plume impinges at a single distance x_i. The trajectories of plume segments are governed by the distribution of downdraft velocities whose mean is 0.5 w_*; thus the plume impingement distance for a single realization can vary from o to ∞. However, it is reasonable that these distances are distributed around x_i given by equation (61). With this physical picture of plume behaviour in convective conditions, it is not necessary to think in terms of an effective plume height. The actual mechanics of using x_i in a dispersion model will be described in the next section.

Weil's (1979) observations indicate that the plume breakup model might be appropriate in certain cases. In view of this, it is worthwhile to describe briefly the breakup model suggested by Weil. According to him, the final plume rise in convective conditions is given by

$$z_{pf} = 1.6 \frac{F_o^{1/3}}{u} (3.5 \; x_*)^{2/3} \tag{62}$$

The breakup distance x_* is obtained by equating the plume dissipation rate to the ambient turbulent dissipation rate which was assumed to be

$$\varepsilon = 0.5 \; q \tag{63}$$

$$q = \frac{g}{T} \; H_o \tag{64}$$

The resultant formula for x_* is

$$x_* = 0.65 \; F_o^{2/5} \; u^{3/5}/q^{3/5} \tag{65}$$

Weil (1979) obtained good results by assuming that $\rho C_p H_o$ = 0.31 times the insolation rate.

In summary, there is no general agreement on the plume rise equation to use in convective conditions.

This is related to the difficulty in measuring or for that matter defining plume rise when the plume is looping. For the time being, one has to be satisfied with indirect verification of the equations; comparison of concentration predictions with observations will determine the "correctness" of the plume rise formulation used in the dispersion model.

4. CONVECTIVE DISPERSION MODEL

4.1 PLUME BEHAVIOUR

Plumes emitted into the convective boundary layer exhibit the slow up and down motion commonly referred to as "looping". This behaviour is associated with the vertical motions inside the updrafts and downdrafts which extend through the depth of the mixed layer. These regions of vertical motion are advected past the stack at the speed of the mean wind. Pollutants emitted into a downdraft initially move upward as a result of its buoyancy. However, at some distance the downdraft velocity become greater than the upward buoyant velocity and the plume segment starts travelling towards the ground. On the other hand, plume segments caught in updrafts travel upward. The downwind advection of these plume segments travelling in opposite vertical directions gives rise to the illusion of a sinuous plume; hence the term "looping".

Pollutants caught in updrafts would start moving downward at the top of the mixed layer where the vertical flow changes direction. Thus they would be diluted considerably before they hit the ground. On the other hand, pollutants travelling in the relatively less turbulent downdrafts would be more concentrated when they reach groundlevel. Therefore, it would be reasonable to assume that the groundlevel concentration distribution is determined by plume segments emitted into downdrafts.

The vertical mixing in the convective PBL is accomplished primarily by large energetic eddies whose velocities scale with w_* and whose dimensions scale with z_i; the relevant time scale τ_m for dispersion is then z_i/w_*. The non-dimensional distance X from the source which conveys information about the extent of vertical mixing can be readily defined as

$$X \equiv \frac{w_*}{z_i} \frac{x}{u} \tag{66}$$

where x is the distance from the source. Note that X is the ratio of the travel time x/u to the mixing time τ_m. At small X, the plume would not be affected by the mixing action of the large eddies. At large X (X >3), the pollutants would be well mixed through the depth of the PBL.

4.2 THE MODEL

With the preliminaries of the preceding section, the dispersion model can now be described for convective conditions. In the following development it will be convenient to deal initially with the crosswind integrated concentration $\hat{C}^y$ given by

$$\hat{C}^y(t) = \int_{-\infty}^{+\infty} C(x, y, o, t)dy \tag{67}$$

Figure 5 shows a schematic of the physical system being considered. Based on visual evidence of the behaviour of the looping plume it is assumed that a plume segment spreads about its centerline as it is moved bodily up and down by the vertical motion in the convective updrafts and downdrafts. As these downdrafts (or updrafts) have relatively long lifetimes (Lamb 1978b), it is reasonable to assume that a plume segment emitted into a downdraft will remain in it until it impinges on the ground. Figure 5 illustrates such a situation. Note that the vertical velocity of the plume can be resolved into an upward acting buoyant velocity and an opposing downdraft velocity which eventually brings the plume segment down to the ground. As the emission point

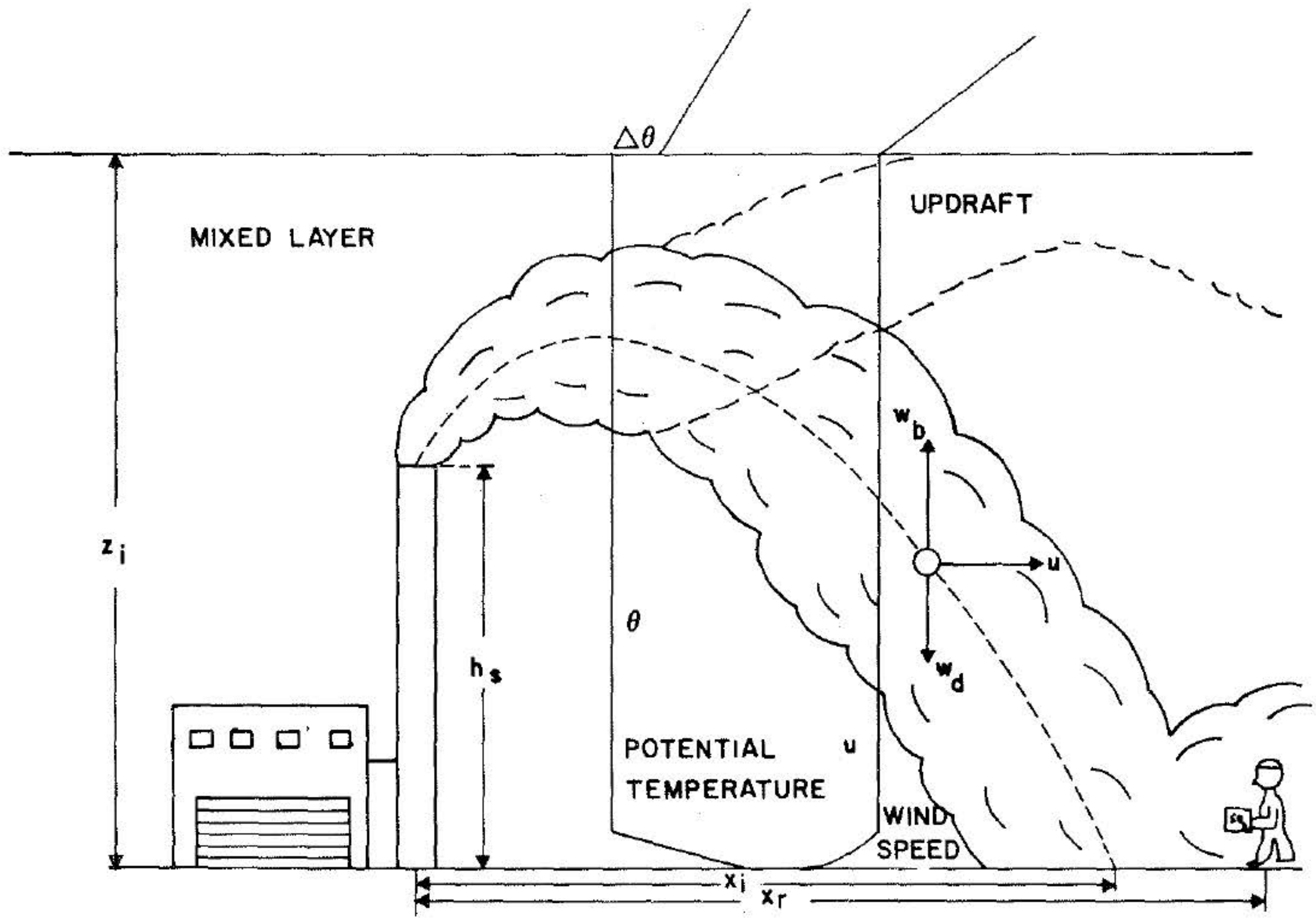

Figure 5. Plume behaviour in convective conditions.

is taken to be well above the shear dominated surface layer, most of the downward travel of the plume occurs in a region in which the velocity (and potential temperature) is virtually uniform.

Consider a detector whose reading $I(t)$ is given by

$$I(t) = 1.0 \; ; \; \hat{C}^y(t) > 0$$

$$I(t) = 0.0 \; ; \; \hat{C}^y(t) = 0$$

$$\overline{I(t)} = f \tag{68}$$

where $\overline{I(t)}$ denotes a time average of the stationary function $I(t)$. It is easy to see that f at a distance x_r is the fraction of time the plume is detected at groundlevel on the line $x = x_r$. It is reasonable to assume that a majority of plume segments hitting the ground will stay close to the surface as they are advected downwind. As the probability of a plume segment reaching the ground increases with distance from the source, it follows that f would be given by the cumulative probability of plume impingement at distances $x < x_r$. Specifically, if $P_d(x)$ is the probability density of plume impingement at groundlevel, f can be written as

$$f = \int_0^{x_r} P_d(x, \nu)\,dx \tag{69}$$

where ν refers to variables such as stack height and atmospheric turbulence which determine P_d.

The concentration detected at a receptor x_r can in general be expressed as

$$\hat{C}^y \propto \frac{Q}{u\hat{\sigma}(t)} \tag{70}$$

where $\hat{\sigma}(t)$ is the vertical dimension of the plume segment (crosswind integrated) whose mass per unit length is Q/u. Then the time (ensemble) averaged concentration $\overline{C}^y(x_r\ ;\ \nu)$ can be written as

$$\overline{C}^{\,y}(x_r\ ;\ \nu) \propto \overline{\hat{C}^y(x_r,\ t;\ \nu)\,I(t)} \tag{71}$$

Note that it is assumed that $\hat{C}^y(\nu, t)$ is a stationary time series. This means that the time average is equivalent to an ensemble average over concentration values measured during conditions denoted by the parameter ν; ν in turn is a function of stack conditions and atmospheric turbulence. The problems associated with relating predicted ensemble averaged concentrations to measurements averaged over fixed time intervals will be discussed in a later section.

The right hand side of equation (71) is approximated as follows

$$\overline{\hat{C}^y(x_r,\ t;\ \nu)\ I(t)} \simeq \overline{\hat{C}^y(x_r,\ t;\ \nu)}\,.\,\overline{I(t)} \tag{72}$$

$$= C_p(x_r;\ \nu)\,f$$

where

$$C_p \equiv \overline{\left(\frac{Q}{u\hat{\sigma}}\right)} \equiv \frac{Q}{u\sigma} \tag{73}$$

Note that equation (73) defines the "average" plume segment thickness σ. The expression for the ensemble average concentration $\overline{C}^y(x_r;\ \nu)$ becomes

$$\overline{C}^y = \frac{AQ}{u\sigma}\ f \tag{74}$$

where A is a constant to be determined from the subsequent analysis. Equation (74) implies that the concentration time series at x_r is approximated by top-hat profiles; the concentration at x_r is either zero or C_p. This idea was the basis of a successful dispersion model proposed by Davidson and Halitsky (1958) who suggest that observed concentrations do exhibit this top-hat type behaviour.

It can be seen from equation (74) that f is analagous to the term $\exp(-h_e^2/2\sigma_z^2)$ in conventional Gaussian plume dispersion models which also gives information about the probability of observing concentrations at groundlevel. In the present model, the formulation of f is based on the pattern of plume impingement at the ground. As a plume segment can impinge on the earth's surface at any downwind distance ranging from o to ∞, a convenient choice for $P_d(x)$ is the lognormal distribution. The precise form of $P_d(x)$ is not expected to be critical in determining $\overline{C}^y(x_r;\nu)$ as f depends on the integral of the distribution. The expression for f becomes

$$f = \frac{1}{\sqrt{2\pi}\ln s_g} \int_o^{x_r} \exp\left[-\frac{(\ln x - \ln m_g)^2}{2\ln^2 s_g}\right] d(\ln x) \quad (75)$$

where m_g and s_g are the geometric mean and the standard deviation of the lognormal distribution. The discussion of the "touchdown" plume model (see Section 3) suggests that m_g should be proportional to the mean impingement distance x_i. It is recalled that x_i is the solution of equation (61). Studies by Venkatram (1980a) show that the simplest relationship $m_g = x_i$ yields good results. It was also found that s_g could be estimated by using Lamb's (pers. comm.) results on the statistics of convective velocities in the PBL. He found that the magnitude of the downdraft velocity one standard deviation away from the mean (= 0.5 w_*) was approximately 0.75 w_*. This suggested that s_g could be estimated from

$$s_g = \frac{x_i(w_d = 0.5\ w_*)}{x_i(w_d = 0.75\ w_*)} \tag{76}$$

For the cases considered by Venkatram and Vet (1979) s_g was around 2 for a wide range of conditions.

For the behaviour of σ, it is proposed that

$$\sigma/z_i \propto X\ ;\ \text{small } X \tag{77a}$$

$$\sigma/z_i = \text{constant};\ \text{large } X \tag{77b}$$

Equation (77b) reflects the observation that at large X the vertical spread is limited by the capping inversion at z_i. A plausible interpolation between the limits of equation (77) can be written as

$$\sigma/z_i = \left[1 - \exp(-\ 1.5\ X)\right] \tag{78}$$

The constant 1.5 in equation (78) is based on the model testing described by Venkatram and Vet (1979).

The expression for the centerline groundlevel concentration can be written as

$$C(X,\ o,\ o) = \frac{AQf(X)}{u\sigma_y\sigma} \tag{79}$$

The constant A in equation (79) can be determined by noting that the expression for C(x, o, o) should reduce to that corresponding to the well-mixed PBL at large X

$$C(X,\ o,\ o) = \frac{AQ}{u\sigma_y z_i}\ ;\ \text{large } X \tag{80a}$$

$$= \frac{Q}{\sqrt{2\pi}u\sigma_y z_i}\ \text{(well-mixed PBL)} \tag{80b}$$

From equation (80), $A = 1/\sqrt{2\pi}$. Note that equation (80b) implies that the concentration distribution is Gaussian in the crosswind direction, a description which is adequate according to the tank experiments of Willis and Deardorff (1976).

Based on the results of Islitzer (1961) and Willis and Deardorff (1976), the simplest formulation was selected for σ_y

$$\sigma_y = 0.45\ X\ z_i\ ;\ \text{all } X \tag{81}$$

Islitzer's measurements did not extend beyond $X = 0.5$ As partial support for applying his results to much larger X, Moore's (1974) results are cited on the determination of groundlevel σ_y values due to elevated sources. The results corresponding to sampling times of approximately 1 h indicated that σ_y varied linearly up to 14 km which translates roughly to $X = 4$. This behaviour was followed under a wide variety of meteorological conditions. One possible explanation for this enhanced plume spreading is the conversion of vertical kinetic energy of downdrafts into horizontal kinetic energy as the sinking fluid strikes the ground.

It is necessary to point out that the expressions for σ's do not include the effects of self-induced spread due to plume buoyancy. The results of model testing (Venkatram and Vet 1979) indicated that these effects were minor for dispersion under convective situations.

At this point, it is useful to summarize the equations of the convective dispersion model.

$$C(X,\ o,\ o) = \frac{Qf(X)}{\sqrt{2\pi}\sigma_y \sigma u} \tag{82a}$$

$$X \equiv w_* x / z_i u \tag{82b}$$

$$\sigma_y = 0.45\ X\ z_i \tag{82c}$$

$$\sigma = z_i \left[1 - \exp(-1.5 X) \right] \tag{82d}$$

$$f(X) = \frac{1}{\sqrt{2\pi}} \int_{-\infty}^{p} \exp(-t^2/2)\,dt \tag{82e}$$

$$p = \ln(X/X_i)/\ln s_g \tag{82f}$$

$$X_i = w_* x_i / z_i u \tag{82g}$$

The mean impingement distance x_i is the solution of the "touchdown" equation

$$F^{1/3} x_i^{2/3} - w_d x_i + h_s u = 0 \tag{83a}$$

$$w_d = 0.5\, w_* \tag{83b}$$

$$s_g = \frac{x_i(w_d = 0.5\, w_*)}{x_i(w_d = 0.75\, w_*)} \tag{83c}$$

The results described by Venkatram (1980a) indicate that using a constant value of $s_g = 2.0$ yields comparable model predictions.

Note that f(X) is the probability integral which can be readily evaluated using polynomial approximations described in Abramowitz and Stegun (1972) Equation (83a) is cubic in $x_i^{1/3}$ and can be readily solved using standard methods.

Clearly, the model is very simple (not the opposite of sophisticated) in every sense of the word. The input variables can be derived from routinely measured meteorological variables. The mixed layer height can be estimated from temperature soundings. If soundings are not available, eminently acceptable estimates can be obtained from simple mixed layer models such as the one proposed by Carson and Smith (1974). As seen in Section 3, the convective velocity scale w_* can be related to the incoming solar radiation. To emphasize the simplicity of the model, it should be pointed out that rough estimates (within a factor of 2) of ground-level concentrations can be obtained from equation (80b) which reduces to the simple form

$$C(x, o, o) = \frac{0.9\ Q}{w_* z_i x} \tag{84}$$

The reader is referred to Venkatram (1980a) for examples of the application of equation (84).

4.3 EXAMPLE OF APPLICATION TO THE AOSERP AREA

The model described in the previous section has been applied to three independent sets of data. Two of them, reported by Weil (1977) consisted of concentration and meteorological measurements made in the vicinity of the Dickerson and Morgantown power plants situated in Maryland. The third set consisted of measurements made around the INCO nickel smelter in Sudbury, Ontario.

The model was tested with these observations. The results of the comparison were extremely encouraging. For all three sets of data, more than 80% of the predictions were within a factor of 2 of the observations. The coefficients of determination (r^2) for the model testing with the Morgantown and Dickerson data sets were higher than 0.70. This means that more than 70% of the variance of the observations was explained by the model. For the Sudbury observations, the explained variance was 60%. Details of the model testing are described elsewhere (Venkatram 1980a; Venkatram and Vet 1979). For the purpose of this study, it is only necessary to emphasize that the convective dispersion model of this report has been shown to produce good results and has been validated using accepted methods. Thus, the present author has a great deal of confidence in applying the model to the AOSERP area.

The two major point sources in the AOSERP area are the Suncor powerhouse and the Syncrude main stacks. Stack parameters for these sources are reproduced from Walmsley and Bagg (1978) in Table 3. Based on the information in Table 1, two possible meteorological scenarios have been selected to compute groundlevel concentrations associated with emissions from the two major stacks. Table 4 presents the two cases together with the input parameters required for the model. Case 1 corresponds to a moderately cloudy period around noon on a summer day while case 2 refers to conditions on a clear summer day in the AOSERP area. The difference between the two cases is reflected in the values of w_* and z_i which in turn depend on the incoming solar radiation. Note that x_i is very sensitive to w_*; a factor of 1.5 increase in the convective velocities translates into more than a factor of 2 change in x_i for both sources. Recall that the mean impingement distance moves closer to the stack as w_* increases.

Tables 5 and 6 present the computed groundlevel concentrations associated with the Suncor and the Syncrude plants for the chosen meteorological conditions. It is noted that increased convective activity as reflected in the values of w_* and z_i in Case 2 results in higher concentrations close to the source and lower concentrations farther away where the pollutants become well mixed through the deeper convective boundary layer. For both meteorological scenarios considered, the SO_2 concentrations associated with the Suncor powerhouse are relatively high close to the source. For Case 1, the maximum concentration of about 332 $\mu g \cdot m^{-3}$ occurs at 2 km from the stack. For Case 2, the maximum of 511 $\mu g \cdot m^{-3}$ occurs around 1 km from the source. To interpret these predictions relative to the Alberta Air Quality standard

Table 3. Source emission rates and stack characteristics of major sources in the AOSERP area.

Source Name	Suncor powerhouse	Syncrude Main
Stack height (m)	107	183
Stack diameter (m)	5.8	7.9
Exit velocity ($m.s^{-1}$)	17.5	23.7
Exit gas temperature (K)	505	505
SO_2 emission rate ($g.s^{-1}$)	2600	3300
Buoyancy parameter ($m^4 s.^{-3}$) (Ambient temperature = 283 K)	635	1600

Table 4. Model computations for two cases.

Case	Meteorological condition w_* ($m \cdot s^{-1}$)	z_i (m)	u ($m \cdot s^{-1}$)	Source name	Mean impingement distance x_i (m)	Standard deviation of impingement, s_g
1	1.6	1180	6.0	Suncor Powerhouse	3200	2.14
				Syncrude main	6500	2.23
2	2.4	1780	6.0	Suncor Powerhouse	1500	1.95
				Syncrude main	2900	2.01

Table 5. Groundlevel concentrations associated with the Suncor powerhouse during selected meteorological conditions.

Distance from stack (km)	Groundlevel concentration ($\mu g.m^{-3}$) Case 1	Groundlevel concentration ($\mu g.m^{-3}$) Case 2
0.5	112	351
1.0	262	511
2.0	332	367
3.0	295	240
4.0	252	169
5.0	215	128
6.0	186	102
7.0	163	84
8.0	145	72
9.0	131	63
10.0	117	56
11.0	108	50
12.0	100	46
13.0	92	42
14.0	86	39
15.0	80	36

Table 6. Groundlevel concentrations associated with the Syncrude main stack during selected meteorological conditions.

Distance from stack (km)	Groundlevel concentration ($\mu g.m^{-3}$) Case 1	Groundlevel concentration ($\mu g.m^{-3}$) Case 2
0.5	13	50
1.0	51	148
2.0	109	203
3.0	134	184
4.0	141	155
5.0	144	130
6.0	135	112
7.0	131	96
8.0	125	85
9.0	119	76
10.0	112	68
11.0	107	62
12.0	102	57
13.0	97	52
14.0	93	48
15.0	88	46

of 0.2 ppm ($\approx$520 $\mu g.m^{-3}$) averaged over a 0.5 h period, it is necessary to discuss the relationship between model predictions and concentration measurements.

The present model, like most other models, predicts what is referred to as the ensemble averaged concentration. To understand this concept, one must consider a series of concentrations (averaged over 0.5 h) measured under identical "controlling" meteorological conditions. Each measurement is called a member of the ensemble defined by the specified variables of the meteorological state. It is assumed that it is possible to define a meteorological state in terms of PBL variables such as wind speed, solar radiation, and surface roughness. For example, the stability classes in the Pasquill-Gifford system are essentially meteorological states which determine the dispersive ability of the boundary layer. Then, the ensemble average is obtained by averaging over the infinite possible members of the ensemble. For a stationary time series, the time average is equal to the ensemble average. In comparing time averaged concentration observations with model predictions, it is implicitly assumed that the sampling time includes a sufficiently large number of concentration events to treat the observed concentration as an approximation to a stable ensemble average. Although there is often justification for this assumption, it should be realized that the deviation of the observed concentration from the ensemble average can be substantial in certain cases. The expected deviation of the time-averaged concentration C_T from the ensemble averaged concentration C is given by (Tennekes and Lumley 1972)

$$\overline{(C_T - C)^2} = \frac{2\overline{c^2}}{T} \int_0^T \left(1 - \frac{\tau}{T}\right) \rho(\tau) d\tau \qquad (85)$$

where $\overline{c^2}$ is the ensemble concentration variance at the receptor under consideration, and $\rho(\tau)$ is the concentration auto-correlation function. It can be shown (Venkatram 1979) that equation (85) can be approximated by

$$\frac{\overline{(C_T - C)^2}}{\overline{c^2}} \simeq \frac{2(\Gamma - 1)T_i}{T} \tag{86}$$

where T is the averaging time and T_i is the Eulerian time scale controlling dispersion; $\Gamma \equiv C_p/C$ where C_p is the "average" peak concentration of the time series. It is estimated that $\Gamma = 5$ close to an elevated source and $\Gamma = 2$ further downwind (Venkatram 1979) where the concentration is less intermittent. The Eulerian time scales are estimated to range from 60 s in neutral conditions to 300 s under convective conditions. The estimate of T_i for convective conditions is based on the frozen field hypothesis for turbulence (Tennekes and Lumley 1972). A rough estimate for T_i is λ/u where λ is the dominant eddy scale controlling dispersion. It is assumed that $\lambda \propto z_i$; then taking $z_i = 1500$ m and $u = 5$ m.s^{-1} it is found that T_i should be around 300 s. It should be pointed out that there are no direct measurements to verify these estimates.

In order to use equation (86), it will be assumed that, if $T >> T_i$, C_T is not likely to be zero at any time. Then, there is justification in taking C_T to be lognormally distributed (see Csanady 1973). Denoting the left hand side of equation (86) by ε^2, the logarithmic standard deviation σ_l of the distribution can be expressed as

$$\sigma_l = \left[\ln(1 + \varepsilon^2)\right]^{1/2}$$

With this information, the parameters presented in Table 6 can be computed. f_p is the fraction of measurements expected to meet the commonly used factor of 2 criterion for model validation. If it is assumed that the model is perfect and can indeed predict the true ensemble average, and that concentration observations can be made under steady meteorological conditions, Table 7 indicates that, even for this ideal scenario, the stochastic nature of concentration fields limits the ability to predict what is observed. Close to an elevated source ($\Gamma = 5$), only 53% of 0.5 h averaged concentrations are expected to meet the factor of 2 criterion. The situation improves farther downwind where $\Gamma = 2$. As expected, f_p increases with averaging time. For an averaging time of 1 h, 93% of observations can be expected to lie within a factor of 2 when the receptor is some distance away from the point of maximum concentration. It is useful to recall that this problem of model predictability is related to the relatively long time scales of dispersion in convective conditions. Note that T_i determines the duration of a concentration event. Thus, for a fixed averaging time, the long T_i limits the number of independent samples available for averaging. In practical situations, it is not possible to average much beyond an hour due to nonstationarity effects in the slowly evolving planetary boundary layer.

Using the concepts just developed, the probability was computed that the observed concentrations (0.5 h averages) will exceed the Alberta standard of 520 $\mu g.m^{-3}$ under the conditions used for the example presented in Tables 5 and 6. Denoting the model prediction by C and the Alberta standard by C_s, the expression for f_s can be written as

Table 7. Uncertainty of model calculations.

Averaging time (h)	T_i (s)	Γ	f_p
0.5	300	5	0.53
0.5	300	2	0.82
1	300	5	0.66
1	300	2	0.93

f_p = fraction within a factor of 2 of the mean concentration

Stack name	Meteorological conditions	T_i	Γ	ε^2	f_s
Suncor	Case 1	300	5	1.33	0.17
Suncor	Case 1	300	2	0.33	0.14
Suncor	Case 2	300	5	1.33	0.32
Suncor	Case 2	300	2	0.33	0.38
Syncrude	Case 1	300	5	1.33	0.03
Syncrude	Case 1	300	2	0.33	0.00
Syncrude	Case 2	300	5	1.33	0.07
Syncrude	Case 2	300	2	0.33	0.00

f_s = fraction of 0.5 h averages expected to exceed the Alberta standard of 520 $\mu g.m^{-3}$.

$$f_s = \frac{1}{\sqrt{2\pi}} \int_p^{\infty} e^{-t^2/2} dt \qquad (88a)$$

$$p = \frac{\sigma_1}{2} + \ln(C_s/C)/\sigma_1 \qquad (88b)$$

To construct the second part of Table 7, C was taken to be the maximum concentration predicted by the model. For example, C = 332 $\mu g.m^{-3}$ for Case 1 (Table 4) for the Suncor stack. Although the maximum predicted concentration is well below the Alberta standard, 17 out of 100 measurements can be expected to exceed the standard. For Case 2 where the maximum predicted concentration of 511 $\mu g.m^{-3}$ is close to the standard, as much as 38% of the observations can exceed the standard. For the meteorological conditions chosen, SO_2 emission from the Syncrude mainstack is not likely to cause more than 7% exceedances.

The discussion clearly indicates that there is a great deal of uncertainty associated with model predictions even under "ideal" conditions. As most models are far from being caricatures of reality, the actual uncertainty limits are bound to be at least as large as the theoretical estimates. It appears that the factor of 2 criterion is probably stringent enough for most model applications. It should be realized that the "accuracy" of a model cannot be increased beyond the limits set by the stochastic nature of turbulence. It is unrealistic to ask for arbitrary accuracies (say 10%) without taking this into account.

4.4 OUTLINE OF FIELD STUDY IN THE AOSERP AREA

Ideally, a field study should be designed to measure all the variables required for the convective dispersion model. It is useful to list them:

1. Q : emission rate and stack parameters;
2. u : mixed layer wind;
3. z_i: mixed layer height;
4. $w_* \equiv (\frac{g}{T} H_o z_i)^{1/3}$; convective velocity scale;
5. σ_y: standard deviation of groundlevel concentration distribution;
6. σ : vertical thickness of plume; and
7. C(x, y) : groundlevel concentration distribtuion.

The meteorological conditions for the field study should be as close as possible to the ideal situation assumed in constructing the model. Specifically, stationarity and horizontal homogeneity of the meteorological fields are assumed. In the AOSERP area where there are no large water bodies and major terrain changes, it might be reasonably safe to assume that the PBL structure does not change in the horizontal direction. Also, as the mixed layer filters out surface variations with wavelengths less than z_i, the requirements on horizontal homogeneity of the terrain are not very critical. On the other hand, one must make sure that the sampling period of the field study is quasi-steady. The 4 h following local noon are probably the best time for field measurements. One can safely assume that meteorological conditions do not vary during each of the 4 h.

Figure 6 shows a schematic of a possible field setup to measure the model variables listed above. It is necessary to have detailed information on stack conditions during the field study. A Cospec is useful in locating the plume, and is very useful for groundlevel monitoring.

The vertical structure of the boundary layer should be probed as often as possible using a minisonde

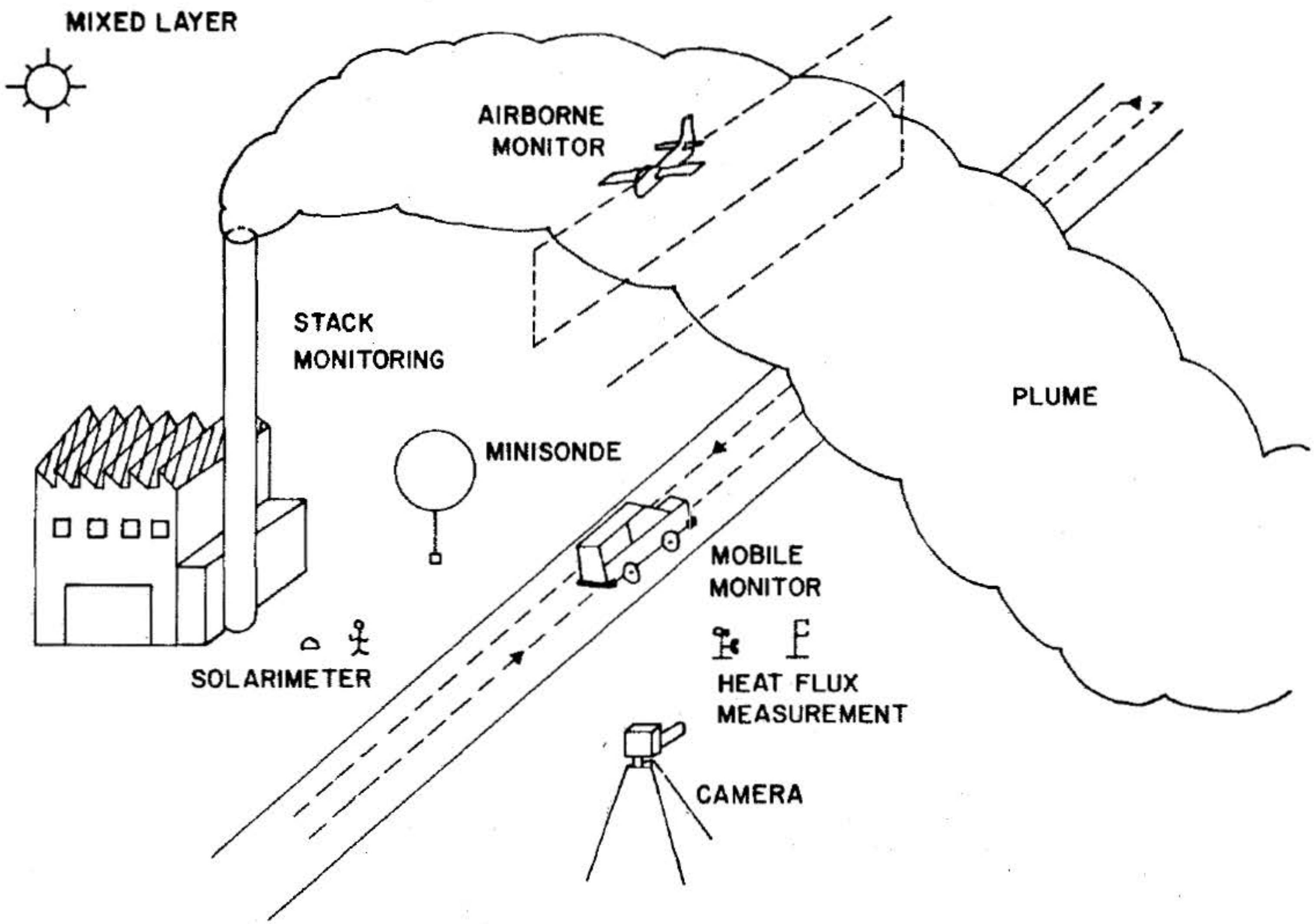

Figure 6. Schematic of experimental set-up to verify the model.

or a pibal. The temperature and velocity profiles obtained from these probes can be used to derive u and z_i. Under convective conditions, a sharp kink in the temperature (and sometimes velocity profile) profile clearly delineates the extent of the mixed layer.

The heat flux H_o appearing in the expression for w_* can be measured using eddy-correlation techniques. However, this type of measurement is local in space and is of dubious value in computing the turbulence affecting the plume. As $w_* \propto H_o^{1/3}$, it is not necessary to use a very accurate method to measure the surface heat flux. Consequently, the incoming solar radiation can serve as a practical surrogate for H_o. Besides being able to be easily measured, solar radiation has the advantage in that it is representative of a large area and is thus more relevant to the dispersion of an elevated plume. An alternative surrogate for H_o is the standard deviation of the temperature fluctuations (see equation 10b). This can be measured readily with simple instrumentation mounted on an aircraft.

Groundlevel concentrations can be measured using mobile monitors. For example, a Sign-X or a Meloy monitor can be fixed to a car which can be driven across the plume. <u>If accessible roads are not available</u> an aircraft can be flown at low heights. A measurement at 30 m is a good approximation to what one would see at groundlevel. It is necessary to make as many traverses as possible across the plume in order to derive a meaningful ensemble averaged concentration profile required for modeling. This also means that sampling time should be as large as the local meteorology will allow. In most situations the sampling time cannot be greater than 1 h. This suggests that the traversing rate should be increased as much as possible either by increasing the speed of the mobile monitor or by using multiple monitors (several cars) on the same traverse path. It can be shown (Venkatram 1980b) that the relative error ε^2 between the measured concentration and the required ensemble average is

$$\varepsilon^2 = \frac{\sigma^2 \Delta t}{T} + \frac{2\sigma^2 \Delta t}{T} \sum_{p=1}^{N-1} \left(1 - \frac{p\Delta t}{T}\right) R(p\Delta t) \qquad (89)$$

where T is the averaging time, Δt is the time interval between traverses, N is the number of traverses, and $R(\tau)$ is the auto-correlation function. The concentration variance at the receptor under consideration is denoted by σ^2. Venkatram (1980b) indicates that at least 10 traverses are needed to reduce ε^2 to an acceptable value. As seen by equation (86), the minimum possible ε^2 is determined by the averaging time T. The effect of stochastic errors is especially important in the derivation of σ_y (see Venkatram 1980b). It is suggested that the technique used to compute σ_y should emphasize the middle of the groundlevel concentration distribution where ε^2 has the smallest values. The best way of doing this is to fit a Gaussian distribution to the composite profile obtained by superimposing all the traverse profiles. It should be pointed out that the σ_y derived from each of the traverses is of little value.

An SO_2 monitor mounted on an aircraft can be used to derive the vertical structure of the concentration profile. While σ_y can be obtained readily from the plume transects, it is much more difficult to interpret and analyze information on the vertical distribution. In the past, there has been a great deal of money spent on aircraft probing of the plume. Consequently, little resources have been used to measure groundlevel concentrations. One should remember that the bottom line is groundlevel concentration; thus, in terms of priorities, the major portion of available resources should be spent on getting an accurate picture at groundlevel. A good knowledge of the vertical structure of the concentration does not necessarily lead to better modelling. The huge expense of an aircraft is often not justifiable when the road system in the study area is adequate.

A camera can be used profitably to provide a visual picture of plume behaviour. This type of semi-qualitative understanding of dispersion is invaluable for modelling. Although the concept of plume rise is not altogether appropriate under convective conditions, photographs can be combined to produce quantitative information on the behaviour of plumes in convective updrafts and downdrafts. For example, it might be possible to get an idea of the mean impingement distance x_i. For a plume with sufficient particulate matter, Weil (1979) suggests that the Lidar is a useful instrument to derive the vertical and horizontal concentration distributions.

When the available resources are substantial, an aircraft can be used to probe the turbulent structure of the PBL. This has been done to a certain extent by Intera (Calgary) under contract from AOSERP. The present author feels that this type of resource hungry study is justified only after a preliminary field study has been conducted, and that modelling and measurement programs should emphasize concentrations rather than sigmas.

5. SUMMARY AND RECOMMENDATIONS

5.1 SUMMARY

Tall stacks are associated with high ground-level concentrations primarily during convective conditions which occur during the daytime hours of summer. In this report, the effects of convective activity on the major elevated sources (Suncor and Syncrude) in the AOSERP study area have been studied. The major objectives fulfilled during the course of the study are described below.

1. The relevant aspects of turbulence in the convective boundary layer have been reviewed. Specifically, the relationship between turbulence in the PBL and the free convection variables such as w_* and z_i have been discussed. The emphasis has been on the fact that w_* derived from the surface heat flux and the mixed layer height was directly related to σ_v and σ_w which determine the dispersion of a plume emitted in the PBL. Several operational methods of deriving w_* have been suggested for dispersion applications. It was demonstrated that a simple thermodynamic model could be used to provide acceptable estimates of z_i. With this background, it was shown that meteorological conditions in the AOSERP area were conducive to the development of buoyancy dominated daytime boundary layers. This demonstrated the need for a convective dispersion model to predict dispersion of the Suncor and Syncrude plumes during summer.

2. Plume rise formulations appropriate for tall stacks were reviewed. In this connection, the 2/3 law for plume rise was derived and it was shown how it could be used to describe plume behaviour in convective conditions. It was found that the concept of "final" plume rise was inappropriate for looping plumes in the unstable PBL. As an alternative, the idea of the mean impingement distance x_i was suggested and it was shown how it could be related to the distribution of plume impingement at groundlevel.
3. A new convective dispersion model was described based on the idea that the groundlevel concentration is determined by the probability density function of plume impingement at the ground. The spread of the plume are functions of w_* and z_i. It was shown that the parameters of the simple model could be related to commonly measured meteorological variables.
4. The convective dispersion model was used to predict concentrations associated with the Suncor and Syncrude plants for plausible meteorological scenarios. It was noted that increased convective activity resulted in higher concentrations close to the source and lower concentrations farther downwind. Results indicated that, for the same meteorological conditions, the emissions from the Suncor powerhouse resulted in higher concentrations than those from the Syncrude mainstack. For the case chosen in the present study, it

was found that the maximum groundlevel concentration due to Suncor stack was very close to the Alberta 0.5 h standard of 520 $\mu g.m^{-3}$ ($\approx$0.2 ppm). This led to the discussion of the expected deviation between model predictions and observations. It was shown that the relatively long time scales of convective turbulence severely limited the predictability of models. This clearly has implications with reference to model applications such as supplementary emission control.

5. An outline was given of a field study designed to verify the convective dispersion model. The importance of making measurements compatible with model requirements was emphasized. All too often, field data are virtually useless for model verification. This is clearly unacceptable in view of the fact that a model represents objective understanding of a physical phenomenon. It is also necessary to make sure that experimental programs assign priorities to measured variables. For dispersion, groundlevel concentration is the primary variable.

5.2 RECOMMENDATIONS

1. The present review indicates that available data are not suitable for verifying the model. Surprisingly, most field studies conducted to date in the AOSERP area have paid little attention to the primary variable: groundlevel concentration. In

the author's opinion, this situation has resulted from a lack of interaction between modellers and experimentalists. It is felt that it is necessary to conduct a fresh field study to rectify this lack of suitable data. The planning of the field study should have a major input from modellers.

2. If it is not already done, routine measurement of incoming solar radiation should be made. Minisondes should be released routinely to measure mixed layer winds and heights. This information can be used to construct a climatology of w_* and z_i which in turn can serve as inputs to long-term models. Visual observation of plumes on a regular basis can also be very useful for modelling.
3. In a recent paper, Strosher and Peters (1980) have presented groundlevel concentrations and the associated meteorological parameters. The authors indicate that dispersion controlled by convective turbulence is important in a number of cases. It is suggested that this data be analyzed with reference to the model presented in this report. It should be pointed out that the data set consists of measurements made at fixed monitors. Thus, most of them do not correspond to centerline concentrations. In view of the stochastic "errors" associated with concentrations measured away from the plume centerline (see 4.3)

model validation is more difficult than with data collected during field studies in which more attention can be given to statistically stable centerline concentrations.

6. REFERENCES CITED

Abramowitz, M. and I. A. Stegun. 1972. Handbook of Mathematical Functions. Dover Publications, Inc., New York. 1046 pp.

Briggs, G.A. 1975. Plume rise predictions. Pages 59-105 in Lectures on Air Pollution and Environmental Impact Analyses, AMS, Boston, Mass.

Carson, D.J. 1973. The development of dry inversion-capped convectively unstable boundary layer. Q. J. R. Met. Soc. 99:450-467.

Carson, D.J. and F.B. Smith. 1974. Thermodynamic model for the development of a convectively unstable boundary layer. Advances in Geophysics. 18A:111-124.

Csanady, G.T. 1956. The rise of a hot smoke plume. Aust. J. Appl. Sci. 7:23-28.

Csanady, G.T. 1973. Turbulent diffusion in the environment. D. Reidel Publishing Company, Dordrecht-Holland. 248 pp.

Davidson, B. and J. Halitsky. 1958. A method of estimating the field of instantaneous ground concentrations from tower bivane data. JAPCA. 7:316-319.

Deardorff, J.W. 1972. Numerical investigation of neutral and unstable planetary boundary layers. J. Atmos. Sci. 29:91-115.

Deardorff, J. W. 1974. Three-dimensional numerical study of the height and mean structure of a heated planetary boundary layer. Boundary-Layer Meteorology. 7:81-106.

Deardorff, J.W. and G.E. Willis. 1975. A parameterization of diffusion into the mixed layer. J. Appl. Met. 14:1451-1458.

Islitzer, N.F. 1961. Short-range atmospheric dispersion measurements from an elevated source. J. Met. 18:443-450.

Kaimal, J.C., J.C. Wyngaard, D.A. Haugen, O.R. Cote and Y. Izumi. 1976. Turbulence structure in the convective boundary layer. J. Atmos. Sci. 33:2152-2169.

Lamb, R.G. 1978. A numerical simulation of dispersion from an elevated point source in the convective boundary layer. Atmospheric Environment. 12:1297-1304.

Lamb, R.G. 1979. The effects of release height on material dispersion in the convective planetary boundary layer. Pages 27-33 in preprint volume of the 4th Symposium on Turbulence, Diffusion and Air Pollution, Reno, Nevada, Jan. 15-18.

Longley, R.W. and B. Janz. 1979. The climatology of the Alberta Oil Sands Environmental Research Program Study Area. Prep. for the Alberta Oil Sands Environmental Research Program by Fisheries and Environment Canada, Atmospheric Environment Service. AOSERP Report 39. 102 pp.

Mahrt, L. and D.H. Lenschow. 1976. Growth dynamics of the convectively mixed layer. J. Atmos. Sci. 33:41-51.

Moore, D.J. 1974. A simple boundary-layer model for predicting time mean ground-level concentrations emitted from tall chimneys. Paper presented for ordinary meeting of the Institution (Thermodynamics and Fluid Mechanics group) in London.

Panofsky, H.A., H. Tennekes, D.H. Lenschow and J.C. Wyngaard. 1977. The characteristics of turbulent velocity components in the surface layer under convective conditions. Boundary-Layer Meteorology. 11:355-361.

Plate, E. 1972. Aerodynamics of atmospheric boundary layers. A.E.C. Critical Review Series (TID -24565).

Strosher, M.M. and R. Peters. 1980. Meteorological factors causing SO_2 events from a point source with implications for atmospheric modelling. AMS/APCA Second Joint Conference on Applications of Air Pollution Meteorology, New Orleans, Louisiana, March 24-27.

Tennekes, H. 1973. A model for the dynamics of the inversion above a convective boundary layer. J. Atmos. Sci. 30:558-567.

Tennekes, H. and J.L. Lumley. 1972. A First Course in Turbulence. The MIT Press, Cambridge, Mass. 300 pp.

Tennekes, H. and A.P. van Ulden. 1974. Short-term forecasts of temperature and mixing height on sunny days. Symposium on Atmospheric Diffusion and Air Pollution, (A.M.S.) Santa Barbara, Calif. 35-40.

Venkatram, A. 1977. Internal boundary layer development and fumigation. Atmospheric Environment, 11:479-482.

Venkatram, A. 1978. Estimating the convective velocity scale for diffusion applications. Boundary-Layer Meteorology 15:447-452.

Venkatram, A. 1979. The expected deviation of observed concentrations from predicted ensemble means. Atmospheric Environment 13:1547-1549.

Venkatram, A. 1980a. Dispersion from an elevated source in a convective boundary layer. Atmospheric Environment 14:1-10.

Venkatram, A. 1980b. Model predictability with reference to concentrations associated with point sources. Paper presented at the Joint Conference on Applications of Air Pollution Meteorology, New Orleans, Louisiana, March 24-27, 1980.

Venkatram, A. and R. Vet. 1979. Modeling of dispersion from tall stacks. Paper presented at the NATO/CCMS Conference on Air Pollution Modeling, October 1979, Rome, Italy.

Walmsley, J.L. and D.L. Bagg. 1978. Calculations of annual averaged sulphur dioxide concentrations at ground level in the AOSERP study area. Prep. for the Alberta Oil Sands Environmental Research Program by Fisheries and Environment Canada, Atmospheric Environment Service. AOSERP Report 19. 40 pp.

Weil, J.C. 1977. Evaluation of the Gaussion plume model at Maryland power plants. Martin Marietta Corporation, Baltimore, Maryland. Report No. PPSP-MP-16.

Weil, J.C. 1979. Assessment of plume rise and dispersion models using Lidar data. Environmental Center, Martin Marietta Corporation, Baltimore, Maryland. Report No. PPSP-MP-24. 30 pp.

Weil, J.C. and D.P. Hoult. 1973. A correlation of ground-level concentrations of sulfur-dioxide downwind of the Keystone Stacks. Atmospheric Environment. 7:707-721.

Willis, G.E. and J.W. Deardorff. 1976. A laboratory model of diffusion into the convective planetary boundary layer. Quart. J.R. Met. Soc. 102:427-445.

Wyngaard, J.C. 1973. On surface layer turbulence. Pages 101-148 in Workshop in Micrometeorology, A.M.S. Boston.

Wyngaard, J.C., O.R. Cote and Y. Izumi. 1971. Local free convection, similarity, and the budgets of shear stress and heat flux. J. Atmos. Sci. 28:1171-1182.

Wyngaard, J.C., S.P.S. Arya and O.R. Cote. 1974. Some aspects of the structure of convective planetary boundary layers. J. Atmos. Sci. 31:747-754.

7. APPENDIX

7.1 LIST OF SYMBOLS

u', v', w'	Fluctuating wind components in the longitudinal, lateral and vertical directions
T	Mean temperature
θ'	fluctuating temperature
ρ	density of air
H_o	surface kinematic heat flux
(g/T)	buoyancy parameter
k	von Karman's constant
z	height above ground
z_i	height of mixed layer
L	Monin-Obukhov length = $-u_*^3/k(gT)H_o$
u_*, T_*	scaling velocity and temperature for the surface shear layer
u_f, T_f	scaling velocity and temperature for the free-convection layer
w_*, θ_*	scaling velocity and temperature for the mixed layer

8. AOSERP RESEARCH REPORTS

1.		AOSERP First Annual Report, 1975
2.	AF 4.1.1	Walleye and Goldeye Fisheries Investigations in the Peace-Athabasca Delta--1975
3.	HE 1.1.1	Structure of a Traditional Baseline Data System
4.	VE 2.2	A Preliminary Vegetation Survey of the Alberta Oil Sands Environmental Research Program Study Area
5.	HY 3.1	The Evaluation of Wastewaters from an Oil Sand Extraction Plant
6.		Housing for the North--The Stackwall System
7.	AF 3.1.1	A Synopsis of the Physical and Biological Limnology and Fisheries Programs within the Alberta Oil Sands Area
8.	AF 1.2.1	The Impact of Saline Waters upon Freshwater Biota (A Literature Review and Bibliography)
9.	ME 3.3	Preliminary Investigations into the Magnitude of Fog Occurrence and Associated Problems in the Oil Sands Area
10.	HE 2.1	Development of a Research Design Related to Archaeological Studies in the Athabasca Oil Sands Area
11.	AF 2.2.1	Life Cycles of Some Common Aquatic Insects of the Athabasca River, Alberta
12.	ME 1.7	Very High Resolution Meteorological Satellite Study of Oil Sands Weather: "A Feasibility Study"
13.	ME 2.3.1	Plume Dispersion Measurements from an Oil Sands Extraction Plant, March 1976
14.		
15.	ME 3.4	A Climatology of Low Level Air Trajectories in the Alberta Oil Sands Area
16.	ME 1.6	The Feasibility of a Weather Radar near Fort McMurray, Alberta
17.	AF 2.1.1	A Survey of Baseline Levels of Contaminants in Aquatic Biota of the AOSERP Study Area
18.	HY 1.1	Interim Compilation of Stream Gauging Data to December 1976 for the Alberta Oil Sands Environmental Research Program
19.	ME 4.1	Calculations of Annual Averaged Sulphur Dioxide Concentrations at Ground Level in the AOSERP Study Area
20.	HY 3.1.1	Characterization of Organic Constituents in Waters and Wastewaters of the Athabasca Oil Sands Mining Area
21.		AOSERP Second Annual Report, 1976-77
22.		Alberta Oil Sands Environmental Research Program Interim Report to 1978 covering the period April 1975 to November 1978
23.	AF 1.1.2	Acute Lethality of Mine Depressurization Water on Trout Perch and Rainbow Trout
24.	ME 1.5.2	Air System Winter Field Study in the AOSERP Study Area, February 1977.
25.	ME 3.5.1	Review of Pollutant Transformation Processes Relevant to the Alberta Oil Sands Area

26.	AF 4.5.1	Interim Report on an Intensive Study of the Fish Fauna of the Muskeg River Watershed of Northeastern Alberta
27.	ME 1.5.1	Meteorology and Air Quality Winter Field Study in the AOSERP Study Area, March 1976
28.	VE 2.1	Interim Report on a Soils Inventory in the Athabasca Oil Sands Area
29.	ME 2.2	An Inventory System for Atmospheric Emissions in the AOSERP Study Area
30.	ME 2.1	Ambient Air Quality in the AOSERP Study Area, 1977
31.	VE 2.3	Ecological Habitat Mapping of the AOSERP Study Area: Phase I
32.		AOSERP Third Annual Report, 1977-78
33.	TF 1.2	Relationships Between Habitats, Forages, and Carrying Capacity of Moose Range in northern Alberta. Part I: Moose Preferences for Habitat Strata and Forages.
34.	HY 2.4	Heavy Metals in Bottom Sediments of the Mainstem Athabasca River System in the AOSERP Study Area
35.	AF 4.9.1	The Effects of Sedimentation on the Aquatic Biota
36.	AF 4.8.1	Fall Fisheries Investigations in the Athabasca and Clearwater Rivers Upstream of Fort McMurray: Volume I
37.	HE 2.2.2	Community Studies: Fort McMurray, Anzac, Fort MacKay
38.	VE 7.1.1	Techniques for the Control of Small Mammals: A Review
39.	ME 1.0	The Climatology of the Alberta Oil Sands Environmental Research Program Study Area
40.	WS 3.3	Mixing Characteristics of the Athabasca River below Fort McMurray - Winter Conditions
41.	AF 3.5.1	Acute and Chronic Toxicity of Vanadium to Fish
42.	TF 1.1.4	Analysis of Fur Production Records for Registered Traplines in the AOSERP Study Area, 1970-75
43.	TF 6.1	A Socioeconomic Evaluation of the Recreational Fish and Wildlife Resources in Alberta, with Particular Reference to the AOSERP Study Area. Volume I: Summary and Conclusions
44.	VE 3.1	Interim Report on Symptomology and Threshold Levels of Air Pollutant Injury to Vegetation, 1975 to 1978
45.	VE 3.3	Interim Report on Physiology and Mechanisms of Air-Borne Pollutant Injury to Vegetation, 1975 to 1978
46.	VE 3.4	Interim Report on Ecological Benchmarking and Biomonitoring for Detection of Air-Borne Pollutant Effects on Vegetation and Soils, 1975 to 1978.
47.	TF 1.1.1	A Visibility Bias Model for Aerial Surveys for Moose on the AOSERP Study Area
48.	HG 1.1	Interim Report on a Hydrogeological Investigation of the Muskeg River Basin, Alberta
49.	WS 1.3.3	The Ecology of Macrobenthic Invertebrate Communities in Hartley Creek, Northeastern Alberta
50.	ME 3.6	Literature Review on Pollution Deposition Processes
51.	HY 1.3	Interim Compilation of 1976 Suspended Sediment Date in the AOSERP Study Area
52.	ME 2.3.2	Plume Dispersion Measurements from an Oil Sands Extraction Plan, June 1977

53.	HY 3.1.2	Baseline States of Organic Constituents in the Athabasca River System Upstream of Fort McMurray
54.	WS 2.3	A Preliminary Study of Chemical and Microbial Characteristics of the Athabasca River in the Athabasca Oil Sands Area of Northeastern Alberta
55.	HY 2.6	Microbial Populations in the Athabasca River
56.	AF 3.2.1	The Acute Toxicity of Saline Groundwater and of Vanadium to Fish and Aquatic Invertebrates
57.	LS 2.3.1	Ecological Habitat Mapping of the AOSERP Study Area (Supplement): Phase I
58.	AF 2.0.2	Interim Report on Ecological Studies on the Lower Trophic Levels of Muskeg Rivers Within the Alberta Oil Sands Environmental Research Program Study Area
59.	TF 3.1	Semi-Aquatic Mammals: Annotated Bibliography
60.	WS 1.1.1	Synthesis of Surface Water Hydrology
61.	AF 4.5.2	An Intensive Study of the Fish Fauna of the Steepbank River Watershed of Northeastern Alberta
62.	TF 5.1	Amphibians and Reptiles in the AOSERP Study Area
63.	ME 3.8.3	Analysis of AOSERP Plume Sigma Data
64.	LS 21.6.1	A Review and Assessment of the Baseline Data Relevant to the Impacts of Oil Sands Development on Large Mammals in the AOSERP Study Area
65.	LS 21.6.2	A Review and Assessment of the Baseline Data Relevant to the Impacts of Oil Sands Development on Black Bears in the AOSERP Study Area
66.	AS 4.3.2	An Assessment of the Models LIRAQ and ADPIC for Application to the Athabasca Oil Sands Area
67.	WS 1.3.2	Aquatic Biological Investigations of the Muskeg River Watershed
68.	AS 1.5.3 AS 3.5.2	Air System Summer Field Study in the AOSERP Study Area, June 1977
69.	HS 40.1	Native Employment Patterns in Alberta's Athabasca Oil Sands Region
70.	LS 28.1.2	An Interim Report on the Insectivorous Animals in the AOSERP Study Area
71.	HY 2.2	Lake Acidification Potential in the Alberta Oil Sands Environmental Research Program Study Area
72.	LS 7.1.2	The Ecology of Five Major Species of Small Mammals in the AOSERP Study Area: A Review
73.	LS 23.2	Distribution, Abundance and Habitat Associations of Beavers, Muskrats, Mink and River Otters in the AOSERP Study Area, Northeastern Alberta
74.	AS 4.5	Air Quality Modelling and User Needs
75.	WS 1.3.4	Interim Report on a Comparative Study of Benthic Algal Primary Productivity in the AOSERP Study Area
76.	AF 4.5.1	An Intensive Study of the Fish Fauna of the Muskeg River Watershed of Northeastern Alberta
77.	HS 20.1	Overview of Local Economic Development in the Athabasca Oil Sands Region Since 1961.
78.	LS 22.1.1	Habitat Relationships and Management of Terrestrial Birds in Northeastern Alberta

79.	AF 3.6.1	The Multiple Toxicity of Vanadium, Nickel, and Phenol to Fish.
80.	HS 10.2 & HS 10.1	History of the Athabasca Oil Sands Region, 1980 to 1960's. Volumes I and II.
81.	LS 22.1.2	Species Distribution and Habitat Relationships of Waterfowl in Northeastern Alberta.
82.	LS 22.2	Breeding Distribution and Behaviour of the White Pelican in the Athabasca Oil Sands Area.
83.	LS 22.2	The Distribution, Foraging Behaviour, and Allied Activities of the White Pelican in the Athabasca Oil Sands Area.
84.	WS 1.6.1	Investigations of the Spring Spawning Fish Populations in the Athabasca and Clearwater Rivers Upstream from Fort McMurray; Volume I.
85.	HY 2.5	An intensive Surface Water Quality Study of the Muskeg River Watershed. Volume I: Water Chemistry.
86.	AS 3.7	An Observational Study of Fog in the AOSERP Study Area.
87.	WS 2.2	Hydrogeological Investigation of Muskeg River Basin, Alberta
88.	AF 2.0.1	Ecological Studies of the Aquatic Invertebrates of the Alberta Oil Sands Environmental Research Program Study Area of Northeastern Alberta
89.	AF 4.3.2	Fishery Resources of the Athabasca River Downstream of Fort McMurray, Alberta. Volume 1
90.	AS 3.2	A Wintertime Investigation of the Deposition of Pollutants around an Isolated Power Plant in Northern Alberta
91.	LS 5.2	Characterization of Stored Peat in the Alberta Oil Sands Area

These reports are not available upon request. For further information about availability and location of depositories, please contact:

Alberta Oil Sands Environmental Research Program
15th Floor, Oxbridge Place
9820 - 106 Street
Edmonton, Alberta
T5K 2J6